bioRxiv preprint doi: https://doi.org/10.1101/2023.12.29.573596; this version posted December 29, 2023. The copyright holder for this preprint (which was not certified by peer review) is the author/funder, who has granted bioRxiv a license to display the preprint in perpetuity. It is made available under aCC-BY-NC 4.0 International license.

Single-molecule detection and super-resolution imaging with a portable and adaptable 3D-printed microscopy platform (Brick-MIC)

Gabriel G. Moya Muñoz[1,+], Oliver Brix[1,+], Philipp Klocke[1], Nicolas D. Wendler[1], Eitan Lerner[2,3], Niels Zijstra[1], Thorben Cordes[1,*]

[1]Physical and Synthetic Biology, Faculty of Biology, Ludwig-Maximilians Universität München, Planegg-Martinsried, Germany
[2]Department of Biological Chemistry, The Alexander Silberman Institute of Life Sciences, Faculty of Mathematics Science, The Edmond J.Safra Campus, The Hebrew University of Jerusalem, Jerusalem 9190401, Israel
[3]The Center for Nanoscience and Nanotechnology, The Hebrew University of Jerusalem, Jerusalem 9190401, Israel

*corresponding author: cordes@bio.lmu.de
[+]these authors contributed equally to this work

Abstract

Over the past decades, single-molecule spectroscopy and super-resolution microscopy have advanced significantly and by now represent important tools for life science research. Despite rapid progress and ongoing development, there is a growing gap between the state-of-the-art and what is accessible to non-optics specialists, e.g., biologists, biochemists, medical researchers, and labs with financial constraints. To bridge this gap, we introduce Brick-MIC, a versatile and affordable open-source 3D-printed micro-spectroscopy and imaging platform. Brick-MIC enables the integration of various fluorescence imaging techniques with single-molecule resolution within a single platform and enables exchange between different modalities within minutes. In this work, we present three variants of Brick-MIC that facilitate single-molecule fluorescence detection, fluorescence correlation spectroscopy and super-resolution imaging. With the three variants, we were able to observe conformational changes and absolute inter-dye distances in single macromolecules and perform single-molecule localization microscopy (STORM and PAINT) of DNA origami nanostructures. Detailed descriptions of the hardware and software components, as well as data analysis routines are provided, to allow non-optics specialist to operate their own Brick-MIC with minimal effort and investments. We foresee that our affordable, flexible, and open-source Brick-MIC platform will be a valuable tool for many laboratories worldwide.

Introduction

Research in the molecular life sciences, biomedicine and under clinical settings heavily relies on the use of light microscopy[1,2], biophysical techniques[3,4], spectroscopic assays, e.g., PCR[5], ELISA[6], DNA sequencing[7] and many others[8–10]. There is rapid advancement of both the instrumentation and the assays to achieve better spatial- and temporal-resolution or higher sensitivity for various applications including virus detection[11–15]. This progress, however, typically takes place in engineering and (bio)physics labs and it is difficult to benefit from it in applied- or industry research and under clinical settings[1,16]. Reasons for this can be the mere dimensions of a setup, or the

bioRxiv preprint doi: https://doi.org/10.1101/2023.12.29.573596; this version posted December 29, 2023. The copyright holder for this preprint (which was not certified by peer review) is the author/funder, who has granted bioRxiv a license to display the preprint in perpetuity. It is made available under aCC-BY-NC 4.0 International license.

inability to operate it outside of controlled lab conditions, e.g., due to missing temperature control or lack of mechanical stability. Thus, many advanced techniques cannot be used in high biosafety labs, on field trips, research ships, in hospitals, doctor's practices, and other locations outside the lab. Consequently, there is a growing gap between the possibilities of the state-of-the-art in microscopy and spectroscopy and what is accessible to all interested users[16,17]. While there are core facilities for imaging and biophysical techniques, these remain too few, might only provide limited infrequent access or come with the requirement for travel. All this poses fundamental limitations since many biological and medicinal studies require long iterative refinement, samples may have to be studied locally and point-of-care applications using advanced techniques are simply not feasible.[16,17]

In recent years, different research groups and companies have started to bridge this gap by miniaturizing microscopy research platforms and reducing costs of commercial systems. Currently, the available compact microscopy setups offer high spatial- and temporal-resolution or high sensitivity. The setups often utilize commercially available optomechanical components, as has been implemented in the smfBOX[18] and miCUBE[19]. On one hand, despite their performance, these setups cannot be used easily outside of optical laboratories and require significant expertise for setting them up, maintaining them, and operating them – making them less suitable for application-oriented users. On the other hand, Oxford Nanoimager's video-based device is small, powerful, and user-friendly, but is inflexible in terms of microscope modalities[20–22]. Another drawback of all the aforementioned microscopes are high costs, which are well over 100,000 €. On the contrary, 3D-printing with plastic materials has gained popularity to replace expensive optomechanics and parts of the microscope frame. AttoBright, a user-friendly, minimalist, confocal microscope, showed that a 3D-printed setup can facilitate single-molecule detection[23]. It comes, however, with significant limitations in terms of data quality and general adaptability compared to the smfBOX or miCUBE. Another option, the "UC2", a camera-based microscope, represents an adaptable platform for various imaging modalities, including bright field, dark field, and fluorescence microscopy[24]. Although this concept provides high modularity and versatility, it is primarily designed for educational purposes, with a focus on helping users understand a microscope and its construction, rather than providing optimized performance in terms of resolution, sensitivity and stability.

To overcome these challenges, we here introduce an open-source microscopy platform called Brick-MIC, which uses a combination a modular 3D-printed scaffold with a minimal number of optical components. It offers the possibility to realize a variety of (fluorescence) microscopy modalities, e.g., confocal and video detection, fluorescence spectroscopy assays, state-of-the-art single-molecule detection and super-resolution optical imaging using the same platform. The scaffold of the microscope consists of four layers made from 3D-printed plastic material (Figure 1): a sample holder, an excitation layer, a detection layer, and a base plate for the interchangeable excitation and detection layers. All technical drawings and detailed descriptions on how to build and assemble the different Brick-MIC modalities are available with this manuscript. We further provide (compiled) python-based data acquisition and analysis software to perform experiments with different confocal modalities, making the Brick-MIC a true open-source microscopy platform. The only requirement to start your own Brick-MIC is access to a standard, low-cost 3D printer and to purchase of a minimal list of opto-mechanical and optical components.

bioRxiv preprint doi: https://doi.org/10.1101/2023.12.29.573596; this version posted December 29, 2023. The copyright holder for this preprint (which was not certified by peer review) is the author/funder, who has granted bioRxiv a license to display the preprint in perpetuity. It is made available under aCC-BY-NC 4.0 International license.

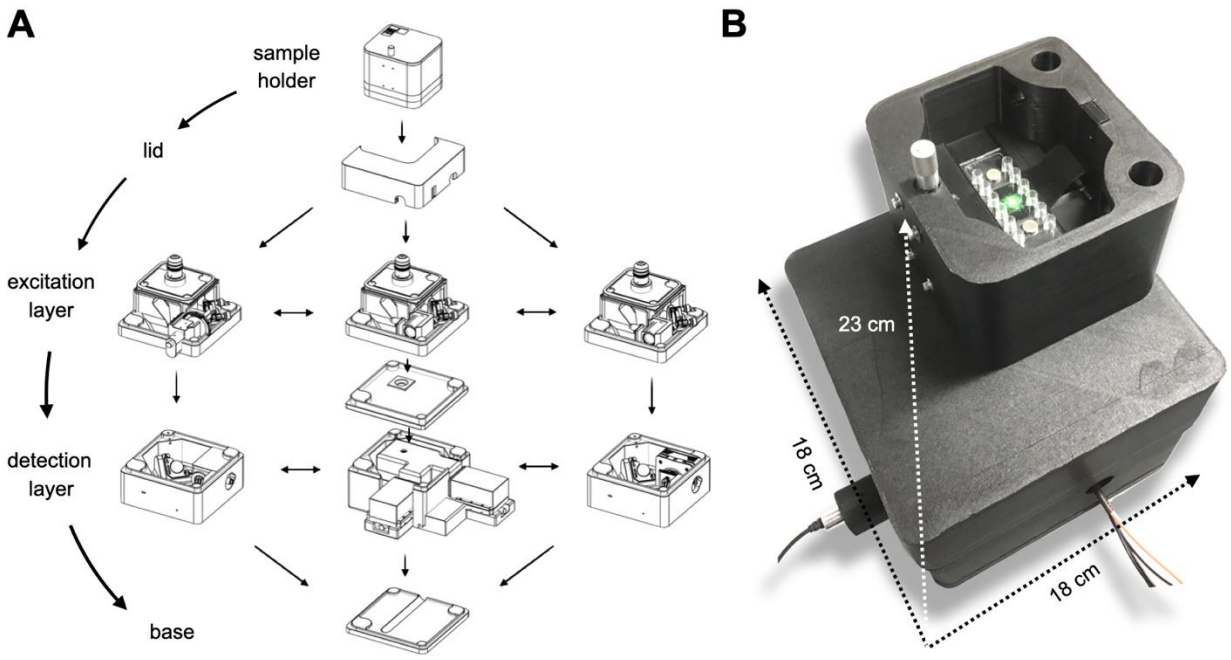

Figure 1. Overview of the adaptable Brick-MIC design. A) The platform uses shape-complementary parts that can be stacked (Lego-like or Japanese "poka yoke"), consisting of different layers: the sample holder, lid, excitation, detection and base layers. The excitation and detection layers are interchangeable, allowing to establish different imaging methods with the same platform and easy exchange of components. B) Photograph of a confocal Brick-MIC modality as used below for analysis of labelled biomolecules in free diffusion (section "Single particle fluorescence detection and fluorescence correlation spectroscopy").

To date, we have established various distinct modalities of the platform, from which we use three as representative examples in this paper. The first is a confocal microscope for single particle detection and fluorescence correlation spectroscopy (FCS[25]), with which we were able to detect individual fluorescent particles, such as freely-diffusing nano-sized fluorescent beads, dye molecules, and labelled bio-molecules of varying sizes. Secondly, we established a two-color confocal microscope that we used for single-molecule Förster resonance energy transfer (smFRET[26,27]) experiments with microsecond alternating-laser excitation (µsALEX[28,29]). Finally, we realized a camera-based microscope that allows standard widefield or darkfield imaging and can be upgraded to an epi-fluorescence microscope for fluorescence and super-resolution imaging via STORM[30,31] and DNA-PAINT[32,33]. We consider our approach a "Swiss-knife" microscope with full flexibility and hope that Brick-MIC will be used inside and outside of research laboratories in the future due to its small size and portability, high stability and state-of-the-art performance.

Results

General considerations for the design of the Brick-MIC platform

Brick-MIC was designed with the philosophy to create a user-friendly, portable and stable, cost-effective and adaptable platform that can be used outside of optical labs under ambient light. To reduce costs and allow robust operation, we established an adaptable microscope body which is fully 3D-printed. This platform is combined

bioRxiv preprint doi: https://doi.org/10.1101/2023.12.29.573596; this version posted December 29, 2023. The copyright holder for this preprint (which was not certified by peer review) is the author/funder, who has granted bioRxiv a license to display the preprint in perpetuity. It is made available under aCC-BY-NC 4.0 International license.

with optical components such as mirrors, filters, etc. from commercial suppliers to establish one microscope modality. The printing templates (https://zenodo.org/records/10441064) and a list of optical and optomechanical components are provided as Supplementary Information (Brick-MIC component list). Once the microscope frames for all modalities are printed, the Brick-MIC platform enables rapid exchange between distinct microscopy modalities within minutes (see Supplementary Video 1). The enclosed sample holder is suitable for the incorporation of microfluidics components, such as Ibidi microfluidics slides and tubing[34], and allows to fix microscope slides with magnets (Supplementary Video 1, 2). A single-axis translation stage, which is integrated into a rack and pinion system, controls the Z-axis position of the coverslip and sample, and ensures high positional stability (Figure 1). The design was tested to generally ensure mechanical stability via an accurate fit of the different layers and vibration dampening by use of thermoplastic Polyurethane (TPU), a resilient and rubber-like material, as the base layer of the microscope (Figure 1). The detection layers of Brick-MIC are all equipped with essential optical components mounted onto piezo motors for convenient alignment of the setup and use of auto-calibration software (see below). Importantly, all modalities of Brick-MIC, presented in this paper require low investment costs between 10.000 and 30.000 €, can be operated with software acquisition packages provided by the respective detector suppliers or with publicly available software (see below), which do not require expensive software licenses, in line with open science practices[17].

Single particle fluorescence detection and fluorescence correlation spectroscopy (FCS)

Confocal microscopy can be used for sensitive detection of (individual) fluorescently-labeled particles and molecules in free diffusion or flow, either via burst detection[35] or FCS[25]. Based on the idea to use Brick-MIC outside of optical labs in biomedical research, clinical diagnostics, or environmental monitoring we established a basic modality with a single cw-laser excitation source and dual-channel detection using photomultipliers, PMTs (Figure 2A/B). The confocal geometry of the setup is achieved using an inversely mounted parabolic collimator that couples the emitted light into an optical fiber (OF). The OF serves as a pinhole (PH) with a diameter related to its core size. The emitted light is captured by a high NA water-immersion microscope objective (60X, NA = 1.2, Olympus – UPLSAPO60XW) and directed by the OF into an external detection box. Here, the emission is spectrally separated via a dichroic mirror (DM) into short (green) and long wavelength emission (red) before reaching two photomultiplier tubes (PMTs; Figure 2B). Signals of both PMTs are read out via an affordable single-photon counter[23] and a bespoke and publicly-available python-based Jupyter Notebook. Importantly, alignment of the setup can be achieved with an automated self-alignment procedure via two piezo mirrors using concentrated solutions of e.g., 100 nM Cy3B (see Online Methods). The self-alignment procedure was directly implemented into the aforementioned Python code and allows exchange of modalities within minutes (see Supplementary Video 1). A notable benefit of this design is the convenient accessibility and interchangeability of the OF, serving as a PH with tunable diameter. This allows for easy modifications to the detection volume of the microscope by selecting optical fibers with varying core diameters, thereby offering enhanced flexibility in tailoring the parameters to specific experimental requirements.

bioRxiv preprint doi: https://doi.org/10.1101/2023.12.29.573596; this version posted December 29, 2023. The copyright holder for this preprint (which was not certified by peer review) is the author/funder, who has granted bioRxiv a license to display the preprint in perpetuity. It is made available under aCC-BY-NC 4.0 International license.

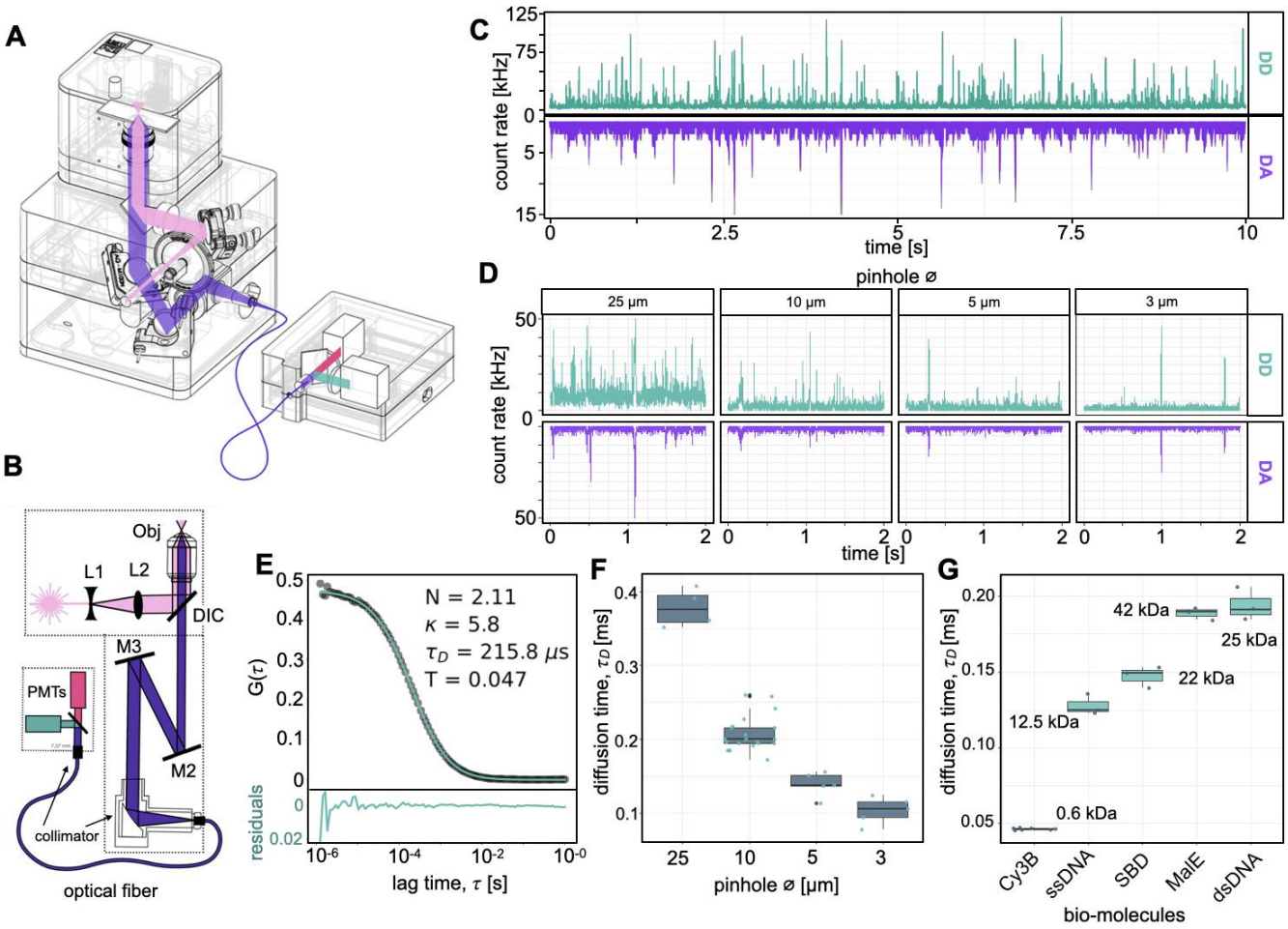

Figure 2. Single molecule detection and fluorescence correlation spectroscopy (FCS) with Brick-MIC. A) CAD model showing Brick-MIC including optical components and the light path (pink: excitation; purple: emission; green and red: spectral split emission after dichroic mirror (DM)). B) Overview of the optical layout. The modality utilizes a single laser diode (pink), which is expanded using a telescope comprising a bi-concave lens (L1) and a plano-convex (L2) and focused into the sample through an objective lens (Obj), for excitation. The emission is collected through the same objective lens and directed via a pair of mirrors on piezo-directed optical mounts (M2 and M3) through an inversely mounted reflective collimator, which focuses and couples the emission beam into an optical fiber. The optical fiber directs the coupled emission light into an external detection box, where it is collimated with a fixed-focus reflective collimator for spectral separation by a dichroic mirror and detection by PMTs. Further details are provided in the Online Methods. C) Single molecule time trace of a 100 pM dsDNA sample labeled with Cy3B donor (D) and ATTO647N acceptor (A) dye at a 13 bp inter-dye distance. Individual bursts are recorded in two different acquisition channels under continuous green excitation: donor (DD) and acceptor emission (DA). D) Zoom-in on time traces (max counts: 50 kHz) of 500 nm Tetraspeck-beads (TS) in laminar flow (2.5 µl/s) measured with different core diameters of the OF, which acts as a pinhole. E) Representative FCS curve of a 5 nM solution of a 40-mer dsDNA sample labeled with Cy3B recorded using a 10 µm pinhole core diameter; fit parameters are number of molecules N, geometry parameter κ, diffusion time τ_D and triplet-fraction T (see Online Methods). F) Boxplot showing FCS-based best-fit average diffusion times of a 5 nM solution of a 40-mer dsDNA sample labeled with Cy3B measured using different PH sizes. G) Boxplot showing FCS-based best-fit average diffusion times of different biomacromolecules labeled with Cy3B with different masses and hydrodynamic radii recorded using a 10 µm PH. Additional data is available in Supplementary Figure 1 and 3. Error bars are standard deviations from n > 3 repeats.

Using this setup, we observed single fluorescently-labeled nanoparticles of varying diameters ≥100 nm (Supplementary Video 2) and individual fluorophore-labeled double-stranded DNA (dsDNA) molecules. Diffusional transits of donor-acceptor labeled dsDNA molecules (donor Cy3B, acceptor ATTO647N in 13 bp distance) were clearly visible as coinciding bursts in both detection channels (Figure 2C). Variation of the OF core

bioRxiv preprint doi: https://doi.org/10.1101/2023.12.29.573596; this version posted December 29, 2023. The copyright holder for this preprint (which was not certified by peer review) is the author/funder, who has granted bioRxiv a license to display the preprint in perpetuity. It is made available under aCC-BY-NC 4.0 International license.

size reveals the effect of shrinking excitation volume in fluorescence time traces (Figure 2C). Larger PH sizes, i.e., large detection volumes, show higher and longer signal periods, higher burst detection frequency as well as increased background compared to smaller PH diameters (Figure 2E-E and Supplementary Figure 2).

The high sensitivity of the setup suggests that it can readily be used for FCS measurements. We first tested and quantified parameters of a 5 nM solution of 40mer-dsDNA labeled with Cy3B (Figure 2D/E). Using a home-written analysis script based on jupyter[36,37] (https://github.com/PSBlmu/FCS-analysis), we could extract molecular brightness B, diffusion times, triplet blinking lifetime and their associated amplitude from a standard diffusion and triplet fit (Figure 2D). The average diffusion times of dsDNA were ~100, ~150, and ~200 µs for increasing PH diameters. The use of an OF with a core size diameter of 10 µm resulted in comparable results to those obtained from a custom-built confocal microscope[36,37] which employs a 50 µm PH. The brightness of Cy3B was lower in the Brick-MIC microscope (10 kHz vs. 80 kHz per molecule, Supplementary Figure 3) according to a reduced PH diameter. The analysis of diffusion times of biomolecules with varying masses and hydrodynamic radii revealed that both setups correctly assess the expected trends related to molecular mass differences (except for the non-spherical dsDNA sample; Figure 2G).

Single-molecule FRET and ALEX

FRET and its single-pair equivalent spFRET (or smFRET) have become an established method in the prospering toolkit of integrative structural biology[37–47]. With the smFRET method, it is possible to study biomacromolecules in aqueous solution at ambient temperature, and to identify conformational heterogeneity and sub-populations, measure accurate distances and to characterize conformational changes (kinetic exchange rates)[27,29,36–42,48–54].

As expected from the sensitivity of the setup, it would be possible to use the PMT-version of our microscope (shown in Figure 2) for ratiometric determination of apparent FRET efficiency E* of single donor-acceptor pairs under continuous green excitation (Figure 2C). We note, however, that the sensitivity of the red detection channel was suboptimal and the available dynamic range of E* would be rather limited in comparison to our home-built setups. We thus further optimized the setup for this specific application. As shown in Figure 3, we used the flexibility of Brick-MIC to exchange the excitation layer to contain a reflective collimator as output of a fiber-coupled laser (Figure 3A). This allows the use of any fiber-coupled laser system (i.e., cw, electronically modulated or pulsed) with different combinations of excitation wavelengths. We further improved the detection efficiency of the setup by use of two single-photon avalanche diodes (SPAD, model PDM 50-Micron, MPD) in the detection layer. These serve as single-photon counters and PHs simultaneously due to their small active detection area of 50 µm diameter[23]. As can be seen from the scheme of the optical setup (Figure 3A/B), the design greatly reduces the number of required optical and opto-mechanical components in comparison to standard home-built setups.

Employing this modality in combination with microsecond alternating laser excitation (µsALEX[29]) of fiber-coupled green and red lasers at an alternation rate of 20 kHz (50 µs excitation periods), we observed bursts from individual freely-diffusing FRET-labeled biomolecules (Figure 3C). From these we extracted photon-streams relevant for ratiometric FRET determination (Figure 3D/E, apparent FRET efficiency E*) and apparent fraction of donor brightness (S*) for each single molecule transit through the confocal excitation volume. As shown for MalE, the periplasmic subunit of the maltose permease[55], both conformational states (apo: ligand-free open and holo: ligand-bound closed) and the ligand affinity can be characterized with single protein resolution[50] (Figure 3D). These experiments utilize FRET as a qualitative indicator for conformational changes via E*, e.g., from low to high E* values, i.e., from long to short inter-dye distance, respectively.

bioRxiv preprint doi: https://doi.org/10.1101/2023.12.29.573596; this version posted December 29, 2023. The copyright holder for this preprint (which was not certified by peer review) is the author/funder, who has granted bioRxiv a license to display the preprint in perpetuity. It is made available under aCC-BY-NC 4.0 International license.

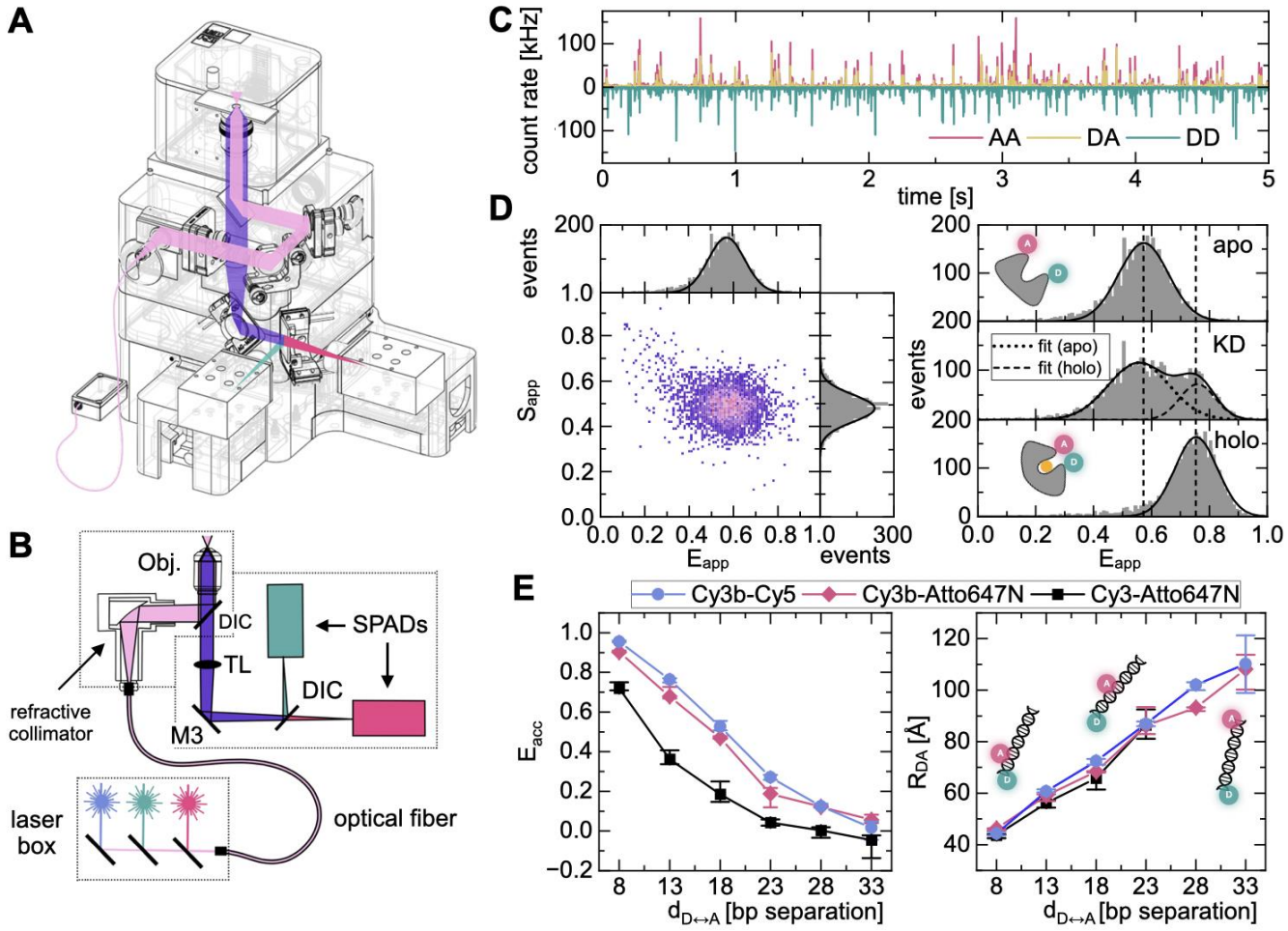

Figure 3. Single-molecule FRET and µsALEX modality. A) CAD model showing all optical components including the light path (pink: excitation; purple: emission; green and red: spectral split emission after the DIC). B) Overview of the optical layout: The modality uses an external laser coupled to the microscope through an OF. In this arrangement, the excitation beam is collimated with a reflective collimator and then focused into the sample through an objective lens. The emission is collected by the same objective lens and is further focused via an achromatic tube lens (TL) directly onto two different single-photon avalanche diodes (SPADs). Spectral separation is achieved by a DM and appropriate bandpass filters for each detector. The M3 Mirror and the DIC in the emission layer are mounted onto piezo-directed mirror holders, which are used to direct the photon stream into each detector channel. C) Time trace of a 100 pM dsDNA sample labeled with Cy3B donor (D) and ATTO647N acceptor (A) dye at a 13 bp inter-dye distance. Individual bursts are recorded in three different acquisition channels: DD (green) for donor excitation and donor emission; AA (red) for acceptor excitation and acceptor emission; and DA (yellow) for donor excitation and acceptor emission. D) Representative ES-histogram of the open conformation of the substrate binding protein MalE (left side). (Right side) Observation of different conformational states of MalE (open, closed, and K_D conditions) for apo (no substrate), holo (100 µM maltose), and K_D (1µM maltose). E) Determination of accurate FRET efficiency values and corresponding distances (R_{DA}) using a DNA ladder for different dye combinations.

We also assessed the ability of the setup to determine accurate FRET efficiencies, E, via correction of E* for all setup-dependent parameters, i.e., spectral crosstalk for donor leakage α, acceptor direct excitation δ, normalization of detection and quantum yield differences of acceptor and donor γ and normalization of excitation intensities and absorption cross sections of acceptor and donor dye ß, to obtain inter-dye distances, R_{DA}, using established procedures[37,38,42]. We compared the E values for an inter-dye base-pair (bp) separation of DNA ladder samples with different distances (in five bp steps) between the donor and acceptor dyes, ranging from 8 to 33 bp. The dependency of E as a function of bp separation differs for the three dye-pairs studied due to differing

bioRxiv preprint doi: https://doi.org/10.1101/2023.12.29.573596; this version posted December 29, 2023. The copyright holder for this preprint (which was not certified by peer review) is the author/funder, who has granted bioRxiv a license to display the preprint in perpetuity. It is made available under aCC-BY-NC 4.0 International license.

Förster distances. We used values of R_0 known from the literature: Cy3-ATTO647N: R_0 = 5.1 nm[51,52]; Cy3B-ATTO647N: R_0 = 6.7 nm[52–54]; Cy3B-Cy5: R_0 = 7.4 nm (for the latter see Online Methods). Importantly, all E values, which are independent of R_0, are consistent between Brick-MIC and the corresponding experiments performed on a home-built confocal setup[36,37] (Supplementary Figure 4, 5, 12). Furthermore, the derived R_{DA} values of all three dye-combinations are internally consistent and the inter-dye distances derived from the different dye pairs cannot be distinguished within the error margins, except for large distances (> 8 nm) that are outside of the sensitive dynamic range of the FRET approach.

Camera-based light microscopy, single-molecule fluorescence detection and super-resolution imaging

All our investigations show that confocal-based single-molecule detection is possible with a minimal and cost-effective 3D-printed microscope system (Figure 2/3). As a final step, we explored the potential of Brick-MIC for camera-based imaging. Figure 4A shows the developed wide-field epi-fluorescence modality. In this configuration, the excitation layer is linked to the light source via an OF, similar to the aforementioned µsALEX modality. We have, however, also tested the modality with a single laser pointer (data not shown) as was used for the confocal-based setup described in Figure 2.

We then tested the microscope for localization-based super-resolution imaging using STORM[30,31] and DNA-PAINT[32,33] For this we obtained DNA-origami nano-rulers from GATTAquant with a single 95 nm distance (STORM) and two 80 nm distances (DNA-PAINT) between dye attachment positions on the respective origami structure[49]. These fluorescent structures were sparsely immobilized on BSA/BSA-biotin coated surfaces and provided images as shown in the left panels of Figure 4C (epi-fluorescence, Supplementary Video 3/4). Applying thiol-containing photoswitching buffer[30,31] or DNA-imager strands to the solution[33] allowed using the blinking emission of individual labels to construct super-resolved images with the ImageJ plugin Thunderstorm[56]. We found that beads were helpful, but not strictly necessary, as fiducial markers to compensate for lateral drift. Both structures were resolvable, and we obtained a localization precision from isolated dyes or binding sites of ~30 nm FWHM and 65 nm FWHM for STORM and PAINT, respectively (Figure 4D). Importantly, this localization precision was achieved from analyzing 2500 consecutive frames.

While the device was specifically tailored for fluorescence imaging, we also show its use in standard transmission light microscopy or contrast-enhancing techniques such as dark-field and oblique illumination, exemplified by images of Radiolarians recorded with the setup. To obtain these images, minimal modifications of the optical components were required. A LED desktop lamp was used as transmission light, positioned right on top of the sample holder. Additionally, the objective was interchanged for a 20x air objective with a low numerical aperture (NA=0.4, 1-U2B225, Olympus). Darkfield imaging, as well as oblique illumination, was achieved by covering the sample holder with aluminum foil and punching small holes in it with different patterns. For darkfield, a round pattern approximately 5 cm in diameter was used. For oblique illumination, a crescent moon shape was punctured in the foil approximately 3 cm away from the objective's axis.

bioRxiv preprint doi: https://doi.org/10.1101/2023.12.29.573596; this version posted December 29, 2023. The copyright holder for this preprint (which was not certified by peer review) is the author/funder, who has granted bioRxiv a license to display the preprint in perpetuity. It is made available under aCC-BY-NC 4.0 International license.

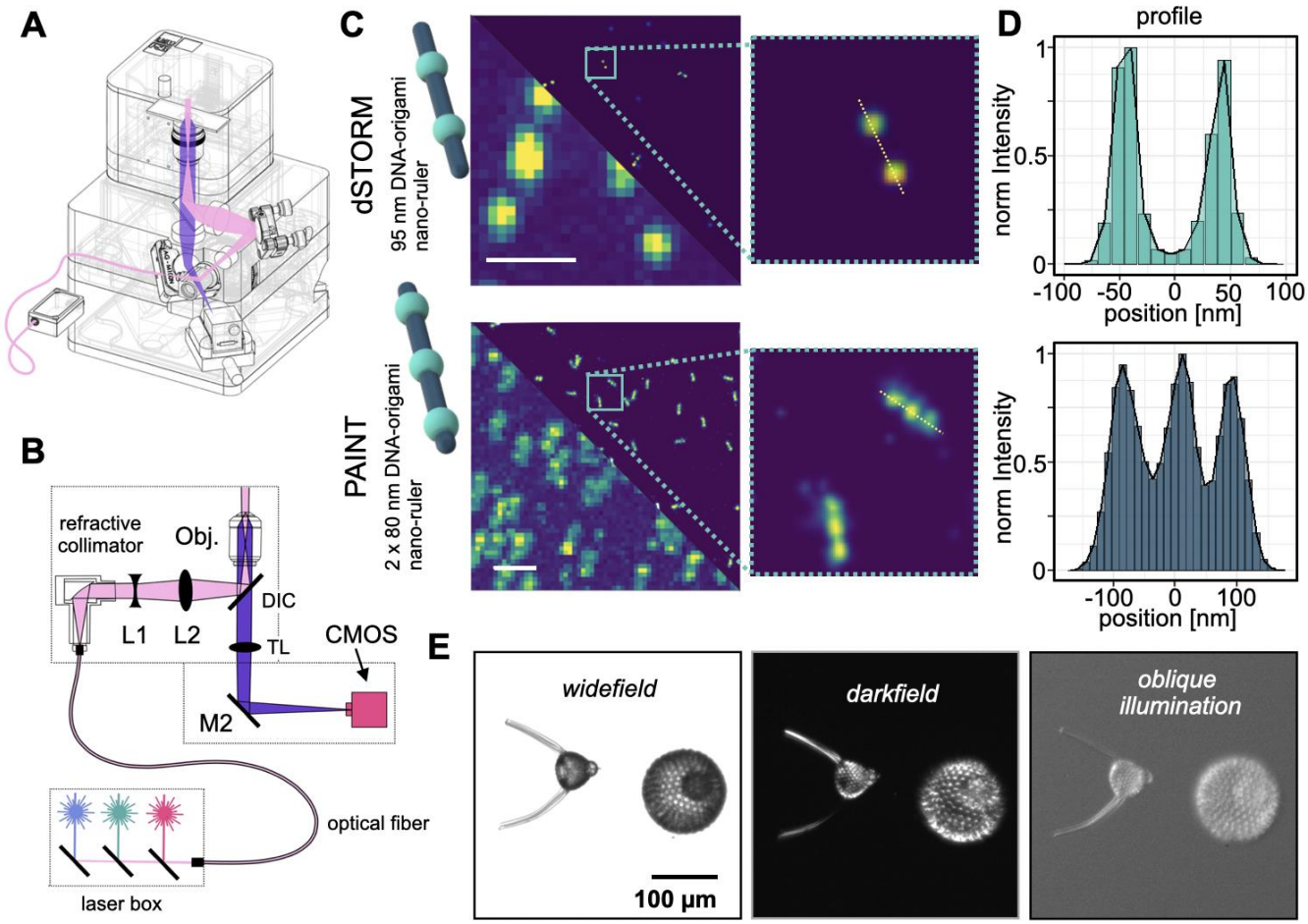

Figure 4. Camera-based light microscopy, single-molecule fluorescence detection and single molecule localization microscopy super-resolution imaging. A) CAD model showing all optical components, as well as the light path (pink: excitation; purple: emission). B) Overview of the optical layout: The modality uses an external laser box coupled to the microscope through an OF. In this arrangement, the excitation beam is collimated with a reflective collimator, which is expanded using a plano-concave lens (L1) and focused with a plano-convex lens (L2) into the back focal plane of the objective lens, resulting in an even illumination of the sample. The emission is collected by the same objective lens and focused via an achromatic tube lens (TL) onto a CMOS camera creating a real image of the sample. C) dSTORM and DNA-PAINT imaging (up and down, respectively) using 2 x 95 nm and 3 x 80 nm DNA-origami nano-ruler structures, respectively. Representative epi-fluorescence image and reconstructed super-resolution single-molecule localization image (left, white line represents 1 µm), with a zoom in (right). D) Representative cross-section profile of a single DNA-origami showing the zoom (yellow dotted line). E) Imaging of Radiolarians using classical contrast methods: transmission light microscopy (left), darkfield illumination (middle), and oblique illumination (right).

Discussion and Conclusion

As shown in this manuscript, Brick-MIC is a high-performance and cost-effective multi-functional microscopy platform that facilitates various state-of-the-art microscopy applications including single-molecule detection and super-resolution microscopy. The modular philosophy of the platform allows for development of additional new modalities not shown here, e.g., TIRF, FLIM or light-sheet microscopy. This versatility might make it a valuable technology platform not only for imaging, but also for a wide range of other scientific directions, e.g., flow cytometry or spectroscopy. Notably, the compact size of the platform offers advantages beyond the confines of the laboratory and that of previous works[17–20,22–24,57] in terms of performance and portability, as it enables

bioRxiv preprint doi: https://doi.org/10.1101/2023.12.29.573596; this version posted December 29, 2023. The copyright holder for this preprint (which was not certified by peer review) is the author/funder, who has granted bioRxiv a license to display the preprint in perpetuity. It is made available under aCC-BY-NC 4.0 International license.

fieldwork research, such as on-site water quality assays, or being deployed in restricted locations such as in high biosafety labs. The portability and small footprint of Brick-MIC make it ideal for conducting research in challenging conditions or real-world scenarios, opening new possibilities for scientific exploration.

We believe that the scientific community and applied users in industry or biomedicine will help us to further improve the technology by testing different optical components of distinct quality, e.g., low vs. high NA objectives. This could further help to balance the requirements for an affordable setup vs. performance. Additionally, extensions of the platform related to temperature control, an autofocus systems for video-microscopy and improved mechanical stability (by use of different 3D-printing materials) could be a topic of future research and engineering of the platform. Other directions would concern the establishment of detector modules where data recording and analysis are more user-friendly, e.g., by use of an action camera or a mobile phone, where data recording and analysis are even easier than demonstrated here.

bioRxiv preprint doi: https://doi.org/10.1101/2023.12.29.573596; this version posted December 29, 2023. The copyright holder for this preprint (which was not certified by peer review) is the author/funder, who has granted bioRxiv a license to display the preprint in perpetuity. It is made available under aCC-BY-NC 4.0 International license.

References

1. Marqués, G., Pengo, T. & Sanders, M. A. Imaging methods are vastly underreported in biomedical research. *eLife* **9**, e55133 (2020).
2. Bond, C., Santiago-Ruiz, A. N., Tang, Q. & Lakadamyali, M. Technological advances in super-resolution microscopy to study cellular processes. *Mol Cell* **82**, 315–332 (2022).
3. Holdgate, G., Embrey, K., Milbradt, A. & Davies, G. Biophysical methods in early drug discovery. *ADMET DMPK* **7**, 222–241 (2019).
4. Miller, H., Zhou, Z., Shepherd, J., Wollman, A. J. M. & Leake, M. C. Single-molecule techniques in biophysics: a review of the progress in methods and applications. *Rep Prog Phys* **81**, 024601 (2018).
5. Zhu, H. *et al.* PCR past, present and future. *Biotechniques* **69**, 317–325 (2020).
6. Sakamoto, S. *et al.* Enzyme-linked immunosorbent assay for the quantitative/qualitative analysis of plant secondary metabolites. *J Nat Med* **72**, 32–42 (2018).
7. Pervez, M. T. *et al.* A Comprehensive Review of Performance of Next-Generation Sequencing Platforms. *Biomed Res Int* **2022**, 3457806 (2022).
8. Dobson, C. M. Biophysical Techniques in Structural Biology. *Annual Review of Biochemistry* **88**, 25–33 (2019).
9. Zheng, Y., Nguyen, J., Wei, Y. & Sun, Y. Recent advances in microfluidic techniques for single-cell biophysical characterization. *Lab Chip* **13**, 2464–2483 (2013).
10. Sun, W., Gao, X., Lei, H., Wang, W. & Cao, Y. Biophysical Approaches for Applying and Measuring Biological Forces. *Advanced Science* **9**, 2105254 (2022).
11. Fang, X., Zheng, Y., Duan, Y., Liu, Y. & Zhong, W. Recent Advances in Design of Fluorescence-based Assays for High-throughput Screening. *Anal Chem* **91**, 482–504 (2019).
12. Reyes, J. L. Z. & Aguilar, H. C. Flow Virometry as a Tool to Study Viruses. *Methods* **134–135**, 87–97 (2018).
13. Brittain, G. C. *et al.* A Novel Semiconductor-Based Flow Cytometer with Enhanced Light-Scatter Sensitivity for the Analysis of Biological Nanoparticles. *Sci Rep* **9**, 16039 (2019).
14. Pebdeni, A. B., Roshani, A., Mirsadoughi, E., Behzadifar, S. & Hosseini, M. Recent advances in optical biosensors for specific detection of E. coli bacteria in food and water. *Food Control* **135**, 108822 (2022).

bioRxiv preprint doi: https://doi.org/10.1101/2023.12.29.573596; this version posted December 29, 2023. The copyright holder for this preprint (which was not certified by peer review) is the author/funder, who has granted bioRxiv a license to display the preprint in perpetuity. It is made available under aCC-BY-NC 4.0 International license.

15. Ahmadsaidulu, S., Banik, O., Kumar, P., Kumar, S. & Banoth, E. Microfluidic Point-of-Care Diagnostics for Multi-disease Detection Using Optical Techniques: A Review. *IEEE Trans Nanobioscience* **PP**, (2023).

16. Power, R. M. & Huisken, J. Putting advanced microscopy in the hands of biologists. *Nat Methods* **16**, 1069–1073 (2019).

17. Hohlbein, J. *et al.* Open microscopy in the life sciences: quo vadis? *Nat Methods* **19**, 1020–1025 (2022).

18. Ambrose, B. *et al.* The smfBox is an open-source platform for single-molecule FRET. *Nat Commun* **11**, 5641 (2020).

19. a) Martens, K. J. A. et al. Visualisation of dCas9 target search in vivo using an open-microscopy framework. *Nat Commun* **10**, 3552 (2019); b) Strack, R. The miCube open microscope. *Nat Methods* **16**, 958 (2019).

20. McNamara, R. P. *et al.* Imaging of surface microdomains on individual extracellular vesicles in 3-D. *Journal of Extracellular Vesicles* **11**, e12191 (2022).

21. McMahon, A. *et al.* High-throughput super-resolution analysis of influenza virus pleomorphism reveals insights into viral spatial organization. *PLOS Pathogens* **19**, e1011484 (2023).

22. Santos, M. F. *et al.* HIV-1-induced nuclear invaginations mediated by VAP-A, ORP3, and Rab7 complex explain infection of activated T cells. *Nat Commun* **14**, 4588 (2023).

23. Brown, J. W. P. *et al.* Single-molecule detection on a portable 3D-printed microscope. *Nat Commun* **10**, 5662 (2019).

24. Diederich, B. *et al.* A versatile and customizable low-cost 3D-printed open standard for microscopic imaging. *Nat Commun* **11**, 5979 (2020).

25. Yu, L. *et al.* A Comprehensive Review of Fluorescence Correlation Spectroscopy. *Frontiers in Physics* **9**, (2021).

26. Deniz, A. A. *et al.* Single-pair fluorescence resonance energy transfer on freely diffusing molecules: Observation of Förster distance dependence and subpopulations. *Proceedings of the National Academy of Sciences* **96**, 3670–3675 (1999).

27. Roy, R., Hohng, S. & Ha, T. A Practical Guide to Single Molecule FRET. *Nat Methods* **5**, 507–516 (2008).

28. Kapanidis, A. N. *et al.* Fluorescence-aided molecule sorting: analysis of structure and interactions by alternating-laser excitation of single molecules. *Proc Natl Acad Sci U S A* **101**, 8936–8941 (2004).

29. Hohlbein, J., Craggs, T. D. & Cordes, T. Alternating-laser excitation: single-molecule FRET and beyond. *Chem. Soc. Rev.* **43**, 1156–1171 (2014).

30. Rust, M. J., Bates, M. & Zhuang, X. Sub-diffraction-limit imaging by stochastic optical reconstruction microscopy (STORM). *Nat Methods* **3**, 793–796 (2006).

bioRxiv preprint doi: https://doi.org/10.1101/2023.12.29.573596; this version posted December 29, 2023. The copyright holder for this preprint (which was not certified by peer review) is the author/funder, who has granted bioRxiv a license to display the preprint in perpetuity. It is made available under aCC-BY-NC 4.0 International license.

31. Heilemann, M. *et al.* Subdiffraction-Resolution Fluorescence Imaging with Conventional Fluorescent Probes. *Angewandte Chemie International Edition* **47**, 6172–6176 (2008).

32. Jungmann, R. *et al.* Single-Molecule Kinetics and Super-Resolution Microscopy by Fluorescence Imaging of Transient Binding on DNA Origami. *Nano Lett.* **10**, 4756–4761 (2010).

33. Jungmann, R. *et al.* Multiplexed 3D cellular super-resolution imaging with DNA-PAINT and Exchange-PAINT. *Nat Methods* **11**, 313–318 (2014).

34. Robb, N. C. *et al.* Rapid functionalisation and detection of viruses via a novel Ca2+-mediated virus-DNA interaction. *Sci Rep* **9**, 16219 (2019).

35. Fries, J. R., Brand, L., Eggeling, C., Köllner, M. & Seidel, C. A. M. Quantitative Identification of Different Single Molecules by Selective Time-Resolved Confocal Fluorescence Spectroscopy. *J. Phys. Chem. A* **102**, 6601–6613 (1998).

36. Gebhardt, C. *et al.* Molecular and Spectroscopic Characterization of Green and Red Cyanine Fluorophores from the Alexa Fluor and AF Series*. *Chemphyschem* **22**, 1566–1583 (2021).

37. Agam, G. *et al.* Reliability and accuracy of single-molecule FRET studies for characterization of structural dynamics and distances in proteins. *Nat Methods* **20**, 523–535 (2023).

38. Hellenkamp, B. *et al.* Precision and accuracy of single-molecule FRET measurements—a multi-laboratory benchmark study. *Nat Methods* **15**, 669–676 (2018).

39. Sisamakis, E., Valeri, A., Kalinin, S., Rothwell, P. J. & Seidel, C. A. M. Accurate single-molecule FRET studies using multiparameter fluorescence detection. *Methods Enzymol* **475**, 455–514 (2010).

40. Lerner, E. *et al.* Toward dynamic structural biology: Two decades of single-molecule Förster resonance energy transfer. *Science* **359**, eaan1133 (2018).

41. Lerner, E. *et al.* FRET-based dynamic structural biology: Challenges, perspectives and an appeal for open-science practices. *eLife* **10**, e60416.

42. Lee, N. K. *et al.* Accurate FRET Measurements within Single Diffusing Biomolecules Using Alternating-Laser Excitation. *Biophysical Journal* **88**, 2939–2953 (2005).

43. Muschielok, A. *et al.* A nano-positioning system for macromolecular structural analysis. *Nat Methods* **5**, 965–971 (2008).

44. Kalinin, S. *et al.* A toolkit and benchmark study for FRET-restrained high-precision structural modeling. *Nat Methods* **9**, 1218–1225 (2012).

bioRxiv preprint doi: https://doi.org/10.1101/2023.12.29.573596; this version posted December 29, 2023. The copyright holder for this preprint (which was not certified by peer review) is the author/funder, who has granted bioRxiv a license to display the preprint in perpetuity. It is made available under aCC-BY-NC 4.0 International license.

45. Hellenkamp, B., Wortmann, P., Kandzia, F., Zacharias, M. & Hugel, T. Multidomain structure and correlated dynamics determined by self-consistent FRET networks. *Nat Methods* **14**, 174–180 (2017).

46. Craggs, T. D. & Kapanidis, A. N. Six steps closer to FRET-driven structural biology. *Nat Methods* **9**, 1157–1158 (2012).

47. Dimura, M. *et al.* Quantitative FRET studies and integrative modeling unravel the structure and dynamics of biomolecular systems. *Curr Opin Struct Biol* **40**, 163–185 (2016).

48. Schuler, B., Lipman, E. A. & Eaton, W. A. Probing the free-energy surface for protein folding with single-molecule fluorescence spectroscopy. *Nature* **419**, 743–747 (2002).

49. Schmied, J. J. *et al.* DNA origami-based standards for quantitative fluorescence microscopy. *Nat Protoc* **9**, 1367–1391 (2014).

50. Peter, M. F. *et al.* Cross-validation of distance measurements in proteins by PELDOR/DEER and single-molecule FRET. *Nat Commun* **13**, 4396 (2022).

51. Bartnik, K. *et al.* A DNA Origami Platform for Single-Pair Förster Resonance Energy Transfer Investigation of DNA-DNA Interactions and Ligation. *J Am Chem Soc* **142**, 815–825 (2020).

52. Holden, S. J. *et al.* Defining the limits of single-molecule FRET resolution in TIRF microscopy. *Biophys J* **99**, 3102–3111 (2010).

53. Ploetz, E. *et al.* Förster resonance energy transfer and protein-induced fluorescence enhancement as synergetic multi-scale molecular rulers. *Sci Rep* **6**, 33257 (2016).

54. Le Reste, L., Hohlbein, J., Gryte, K. & Kapanidis, A. N. Characterization of Dark Quencher Chromophores as Nonfluorescent Acceptors for Single-Molecule FRET. *Biophysical Journal* **102**, 2658–2668 (2012).

55. Mächtel, R., Narducci, A., Griffith, D. A., Cordes, T. & Orelle, C. An integrated transport mechanism of the maltose ABC importer. *Res Microbiol* **170**, 321–337 (2019).

56. Ovesný, M., Křížek, P., Borkovec, J., Svindrych, Z. & Hagen, G. M. ThunderSTORM: a comprehensive ImageJ plug-in for PALM and STORM data analysis and super-resolution imaging. *Bioinformatics* **30**, 2389–2390 (2014).

57. Grabenhorst, L., Trofymchuk, K., Steiner, F., Glembockyte, V. & Tinnefeld, P. Fluorophore photostability and saturation in the hotspot of DNA origami nanoantennas. *Methods Appl Fluoresc* **8**, 024003 (2020).

58. Zhang, L. *et al.* Linker Molecules Convert Commercial Fluorophores into Tailored Functional Probes during Biolabelling. *Angew Chem Int Ed Engl* **61**, e202112959 (2022).

bioRxiv preprint doi: https://doi.org/10.1101/2023.12.29.573596; this version posted December 29, 2023. The copyright holder for this preprint (which was not certified by peer review) is the author/funder, who has granted bioRxiv a license to display the preprint in perpetuity. It is made available under aCC-BY-NC 4.0 International license.

59. de Boer, M. *et al.* Conformational and dynamic plasticity in substrate-binding proteins underlies selective transport in ABC importers. *eLife* **8**, e44652 (2019).

60. Gouridis, G. *et al.* Conformational dynamics in substrate-binding domains influences transport in the ABC importer GlnPQ. *Nat Struct Mol Biol* **22**, 57–64 (2015).

61. Ingargiola, A. *et al.* Multispot single-molecule FRET: High-throughput analysis of freely diffusing molecules. *PLOS ONE* **12**, e0175766 (2017).

62. Förster, Th. Zwischenmolekulare Energiewanderung und Fluoreszenz. *Annalen der Physik* **437**, 55–75 (1948).

63. Diekmann, R. *et al.* Characterization of an industry-grade CMOS camera well suited for single molecule localization microscopy – high performance super-resolution at low cost. *Sci Rep* **7**, 14425 (2017).

bioRxiv preprint doi: https://doi.org/10.1101/2023.12.29.573596; this version posted December 29, 2023. The copyright holder for this preprint (which was not certified by peer review) is the author/funder, who has granted bioRxiv a license to display the preprint in perpetuity. It is made available under aCC-BY-NC 4.0 International license.

Acknowledgments

This work was financed by the European Commission (ERC-STG 638536 – SM-IMPORT to T.C.), the Bundesministerium für Bildung und Forschung (KMU grant „quantumFRET“ to T.C.), the Israel Science Foundation (grants 556/22 and 3565/20 to E.L.), NIH (grant R01 GM130942 to E.L. as subaward) and the Center for Nanosicence (CeNS). The authors also thank the Graduate School Life Science Munich (LSM) for support. N.Z. acknowledges a postdoctoral fellowship from the Alexander von Humboldt foundation. We thank C. Gebhardt and K. Schütze for programming support, M. Isselstein for valuable discussions, and J. Schneider and J. Piedra for experimental support. We thank J. Schmied and GATTAquant for the kind gift of the STORM nanoruler.

Author contributions statement

G.G.M. and T.C. designed and conceived the study. G.G.M. conceived and designed the modular platform architecture. G.G.M., O.B., N.Z. and T.C. planned the layout of the microscopes. G.G.M., O.B. and N.Z. built microscopes and conducted experiments. N.D.W. provided samples. P.K. and N.Z. wrote data acquisition and data analysis software, respectively. G.G.M. and O.B. analyzed data, G.G.M. prepared figures. E.L. and T.C. acquired funding. T.C. supervised the study. G.G.M. and T.C. wrote the initial draft of the manuscript, which was reviewed, edited and approved by all authors.

Competing interest statement

G.G.M., O.B., N.Z. and T.C. have submitted a patent for commercialization of the Brick-MIC microscopy platform. G.G.M. and T.C. declare commercial interest in Brick-MIC.

Additional information

Supplementary files including videos and 3D-printing templates are available in a repository under https://zenodo.org/records/10441064.

bioRxiv preprint doi: https://doi.org/10.1101/2023.12.29.573596; this version posted December 29, 2023. The copyright holder for this preprint (which was not certified by peer review) is the author/funder, who has granted bioRxiv a license to display the preprint in perpetuity. It is made available under aCC-BY-NC 4.0 International license.

Online Methods

Sample preparation

DNA sample for FCS and smFRET. Fluorophore-labeled oligonucleotides, as described in ref. [53], were obtained from IBA (Göttingen, Germany). The DNA single strands were annealed using the following protocol: A 100 µL solution of two complementary single-stranded DNAs (ssDNA) at a concentration of 1 µM was heated to 95°C for 4 minutes and then cooled down to 4 °C at a rate of 1 °C/min in an annealing buffer (500 mM sodium chloride, 20 mM TRIS-HCl, and 1 mM EDTA at pH = 8).

Expression and purification of proteins. MalE single and double cysteine variants as well as the SBD2 (T369C) protein[58] were expressed and purified generally following established and published protocols[50,59,60]. For all MalE derivatives the T7/lac bacterial expression vector pET-23b(+) was chosen with a C-terminal His_6-Tag. For SBD2 (T369C) an araBAD based bacterial expression system was selected including a N-terminal His_{10}-Tag extension.

E. coli BL21(DE3)pLysS competent cells were transformed with the respective vector containing the DNA coding sequences for MalE and SBD2 variants. Expression cultures of the transformant cells were started in 2 l LB medium supplemented with carbenicillin (0.1 mg/ml), chloramphenicol (0.05 mg/ml), and 1 % D-glucose and grown at 37 °C until an optical density (OD_{600}) of 0.6 – 0.8 was reached. Subsequently, over-expression was initiated by addition of 0.25 mM isopropyl β-D-1-thiogalactopyranoside (IPTG) for pET-23b(+) and using 0.2% L-arabinose for araBAD. The cells were harvested after 2 h and resuspended in 50 ml lysis buffer (50 mM Tris-HCl pH 8.0, 1 M KCl, 10 % glycerol, 10 mM imidazole) supplemented with 1 mM dithiothreitol (DTT). The collected cells were subjected to a 30-minute incubation at 4°C with 500 µg/ml DNase I, along with one tablet of EDTA-free protease inhibitor cocktail (cOmplete™, Roche) per 50 ml of culture extract. Additionally, 0.2 mM phenylmethylsulfonyl fluoride (PMSF) and 1 mM DTT were included. The cells were then lysed using an ultrasonic homogenizer (Digital Sonifier 250, Branson) equipped with a 5 mm diameter micro-tip probe, with parameters set at 25% amplitude, a total exposure time to ultrasound of 10 minutes, and time lapses of 0.5 seconds for ON/OFF pulse switches. Coarse cell debris were removed by centrifugation at 5000 × *g* for 30 min at 4 °C, followed by an ultracentrifugation step at 208,400 × *g* for 1 h at 4 °C to remove insoluble cellular components. The over-expressed proteins were purified by metal affinity chromatography using a Nickel functionalized agarose medium (Ni^{2+}-Sepharose™ 6 Fast Flow, Cytiva), pre-equilibrated with 5 CV lysis buffer. A total of 50 ml cell lysate supernatant was loaded onto 4 ml of the Ni^{2+}-Sepharose™ resin suspension and incubated overnight at 4 °C. Following the immobilization, the proteins were washed twice using two times 5 CV lysis buffer supplemented with 1 mM DTT and 0.2 mM PMSF and eluted with 1 CV elution buffer (50 mM Tris-HCl pH 8.0, 50 mM KCl, 10% glycerol, 250 mM imidazole, 0.2 mM PMSF and 1 mM DTT). To eliminate the excess of imidazole, the pooled protein containing fractions were each dialyzed overnight at 4°C against 100 volumes of dialysis buffer (50 mM Tris-HCl pH 8.0, 50 mM KCl) with the addition of 1 mM DTT, using a 10 kDa MWCO dialysis membrane tubing (SnakeSkin™, ThermoScientific). Next, the dialysis buffer was exchanged with 100 volumes of storage buffer (50 mM Tris-HCl pH 8.0, 50 mM KCl, 50% glycerol) supplemented with 1 mM DTT and the proteins were left to dialyze overnight at 4°C. The obtained proteins were snap frozen in liquid nitrogen and stored at -80°C until further use. The final concentrations were determined at a micro-volume Spectrophotometer (NanoPhotometer® N60, IMPLEN) using molar extinction coefficients of 66350 $l*mol^{-1}*cm^{-1}$ for MalE derivatives and 30370 $l*mol^{-1}*cm^{-1}$ for SBD2.

bioRxiv preprint doi: https://doi.org/10.1101/2023.12.29.573596; this version posted December 29, 2023. The copyright holder for this preprint (which was not certified by peer review) is the author/funder, who has granted bioRxiv a license to display the preprint in perpetuity. It is made available under aCC-BY-NC 4.0 International license.

Labelling and labelled protein purification. The stochastic maleimide labelling and purification followed an already established protocol[50,59,60]. For each labeling reaction 600 µg of protein from frozen stocks were used. His_6-tagged MalE (S352C) and MalE (T36C-S352C) as well as the His_{10}-tagged SBD2 (T369C) were incubated in labelling buffer (MalE variants: 50 mM Tris-HCl pH 7.4, 50 mM KCl; SBD2: 50 mM Tris-HCl pH 7.6, 150 mM NaCl) supplemented with 1 mM DTT to retain the reduced state of the introduced cysteine residues. In a first step, the proteins were immobilized by metal affinity on a Nickel functionalized agarose medium (Ni^{2+}-Sepharose™ 6 Fast Flow, Cytiva), subsequently the maleimide reaction with 25 nmol of Cy3B for MalE (S352C) and SBD2 (T369C) (samples for FCS measurements) or with the combination of 25 nmol of each the Alexa Fluor 555 (ThermoFisher) and the Alexa Fluor 647 (ThermoFisher) for MalE (T36C-S352C; smFRET measurements) was carried out in the protein specific labelling buffer overnight at 4°C. The labeled, resin-bound proteins were washed with 1 CV of the respective labelling buffer and eluted with 500 µl labelling elution buffer (MalE variants: 50 mM Tris-HCl pH 8.0, 50 mM KCl, 500 mM imidazole; SBD2: 50 mM Tris-HCl pH 7.6, 150 mM NaCl, 500 mM imidazole). Following the maleimide labelling, the single, Cy3B labelled proteins were purified by size-exclusion chromatography (ÄKTA pure™ chromatography system, Cytiva; Superdex™ 75 Increase 10/300 GL, Cytiva), the MalE (T36C-S352C) was purified by anion exchange chromatography IEX (ÄKTA pure™ chromatography system, Cytiva; MonoQ™ 5/50 GL column, Cytiva).

Since the IEX purification will be topic of a forthcoming publication, we provide a short synopsis here. For MalE (T36C-S352C), the eluate from the maleimide labelling protocol was prepared for further purification by removal of the remaining KCl and imidazole from the labelling elution buffer that could otherwise interfere with the anion exchange process. This step was done using a Sephadex G-25 medium (PD MiniTrap™ G-25, Cytiva). The labelled protein was then eluted in 1 ml of anion exchange sample buffer (10 mM Tris-HCl pH 7.5). The anion exchange column was set up with a 5-CV H_2O_{dd} wash, a 10- column volume equilibration with anion exchange sample buffer, 10- column volume equilibration with anion exchange elution buffer (10 mM Tris-HCl pH 7.5, 1 M NaCl) and a final 20-column volume equilibration with anion exchange sample buffer. The wash and all equilibrations were done with a 1 ml/ min flow rate. Labelled MalE (T36C-S352C) was loaded onto the column with 0.5 ml/ min, subsequently the resin-bound protein was washed with 10 column volumes anion exchange sample buffer and a 1 ml/ min flow rate. For the consecutive elution a linear increase in anion exchange elution buffer ratio with a slope corresponding to 7.5 mM NaCl per column volume was chosen. The flow rate was adjusted to 0.5 ml/ min. Fractions containing MalE (T36C-S352C) with both fluorophores (Alexa Fluor 555 and Alexa Fluor 647) in nearly stoichiometric amounts were selected and used for further analysis.

Sample immobilization (STORM). For every experiment, an ibidi µ-Slide 8 Well Glass Bottom chamber was used. A single µ-Slide chamber was washed three times with 500 µl of PBS before each experiment. Then, 200 µl of a BSA-biotin solution (1 mg/mL in PBS (140 mM NaCl, 10 mM phosphate buffer, and 3 mM KCl, pH 7.4)) with 100 nm tracking fluorescent beads (TetraSpeck, Thermo Fisher) were added to the µ-Slide chamber and incubated for 10 minutes. The BSA-biotin was removed, and the chamber was carefully washed three times with 500 µl PBS. Next, a 200 µl streptavidin solution (1 mg/mL in PBS) was added to the µ-Slide and incubated for 10 minutes. The streptavidin solution was carefully removed, and the chamber was washed three times with imaging buffer IB (PBS with 10 mM magnesium chloride). A 1-10 µl solution of DNA origami nanorods (Gatta-STORM 94R, Gattaquant) was diluted with 200 µl IB and added to the µ-Slide chamber. The DNA origamis were incubated until

bioRxiv preprint doi: https://doi.org/10.1101/2023.12.29.573596; this version posted December 29, 2023. The copyright holder for this preprint (which was not certified by peer review) is the author/funder, who has granted bioRxiv a license to display the preprint in perpetuity. It is made available under aCC-BY-NC 4.0 International license.

a density of 1/µm^2 was reached. Subsequently, the DNA origami solution was removed, and the chamber was washed three times with 500 µl IB. The photoswitching of the fluorophores during imaging was achieved by adding 500 µl of an oxygen scavenging system buffer[58] (pyranose oxidase at 3 U/mL, catalase at a final concentration of 90 U/mL, and 40 mM glucose in PBS) mixed with 0.1% (v/v) ß-mercaptoethanol.

DNA-PAINT. DNA-PAINT samples were obtained ready to use by Gattaquant (Gatta-PAINT 80RG, Gattaquant, Germany).

3D printing of the Brick-MIC platform. All models were designed and conceived using Onshape version 1.114 - 1.172. 3D printing was carried out using PLATech filament (OLYMPfila) on an Ultimaker +2 Extended fitted with a 0.4 mm nozzle. All models were printed with an infill density of 17%, three layers for outer walls and with a layer height of 0.1 mm. The printing speed was set to 50 mm/sec, and the nozzle temperature was maintained at 210 ºC. To prevent warping, all parts were printed with a brim and without any supports. All models are available as STL file as Supplementary CAD files.

Data Acquisition & Data analysis

µFCS. All samples were studied by positioning the confocal excitation volume into a 100 µL PBS droplet with concentrations ranging from 5 to 10 nM on a coverslip passivated with BSA (1 mg/ml in PBS).

The experimental setup shown in Figure 2 employed a 532 nm wavelength CW laser diode (5 mW output; CPS532, Thorlabs) as excitation light source. The beam underwent filtration through a clean-up filter (FL05532-10 ⌀12.5 mm, Thorlabs), attenuation via a continuous neutral density filter wheel (NDC-50C-2M, Thorlabs), and expansion using a telescope comprising a bi-concave lens (f = -50 mm, KBC043AR.14, Newport) and a plano-convex lens (f = 150 mm, LA1433-A-ML, Thorlabs). A dichroic beam splitter with high reflectivity at 532 nm (ZT532/640rpc, Chroma, USA) separated the excitation and emission beams to and from a high numerical aperture (NA) apo-chromatic objective (60X, NA 1.2, UPlanSAPO 60XO, Olympus, Japan). The emitted fluorescence was collected by the same objective, directed via a mirror into a piezo-directed optical mount (AG-M100N, Newport) through an inversely mounted 12 mm reflective collimator (RC12FC-P01, Thorlabs), which focused and coupled the emission beam into a multimode optical fiber (10 µm fiber core diameter, M64L01, Thorlabs). The fiber directed the emission light into a detection box, where it was collimated with a fixed-focus collimator (F220FC-532, Thorlabs) and then spectrally split into two separate photon streams by a dichroic mirror (ZT640rdc longpass, Chroma, USA). Individual photon streams were filtered with bandpass filters (for the green channel: FF01-582/75-25 ⌀25 mm, Semrock Rochester NY, USA; for the red channel: ET700/75m, Chroma) and detected by two distinct photomultiplier tubes with different spectral sensitivities (for the green channel: H10682-210, Hamamatsu, Japan; for the red channel: H10682-01, Hamamatsu, Japan). The detector outputs for FCS analysis were recorded by a NI-Card PCI-6602 (National Instruments, USA) using LabView data acquisition software from the Weiss laboratory{Citation}. Auto-alignment and binned data recording utilized a counter/timer device module (USB-CTR04, Measurement Computing, USA) with custom-made acquisition software written in Python, available for download as compiled executable or editable python code at https://github.com/klockeph/mcc-daq-acquisition.

bioRxiv preprint doi: https://doi.org/10.1101/2023.12.29.573596; this version posted December 29, 2023. The copyright holder for this preprint (which was not certified by peer review) is the author/funder, who has granted bioRxiv a license to display the preprint in perpetuity. It is made available under aCC-BY-NC 4.0 International license.

Data analysis was performed using a home-written Python script[36] (https://github.com/PSBlmu/FCS-analysis), where the intensity fluctuation of freely diffusing molecules $F(\tau)$ is analyzed via autocorrelation:

$$G(\tau) = \frac{<F(t)F(t+\tau)>}{<F(t)^2>} - 1 \qquad \textbf{eqn. 1}$$

Here, the correlation amplitude $G(\tau)$ describes the self-similarity of the signal in time. Average fluorescence intensities at time points t and later lag times τ are used for analysis. $G(\tau)$ is analyzed with a 3D diffusion model:

$$G(\tau) = \frac{1}{N}\left(1 + \frac{\tau}{\tau_D}\right)^{-1}\left(1 + \frac{\tau}{\tau_D}\cdot\frac{r_0^2}{z_0^2}\right)^{-1/2} \qquad \textbf{eqn. 2}$$

Here, N represents the average number of molecules in the confocal volume, τ_D is the average diffusion time, and r_0, z_0 define the lateral and axial radial distances of the detection volume, which define the geometry parameter $\kappa = \frac{z_0}{r_0}$.

µALEX. All samples for smFRET analysis were measured in a 100 µL PBS droplet with concentrations ranging from 50 to 100 pM on a coverslip passivated with BSA (1 mg/ml in PBS). The experimental setup utilized alternating laser excitation (ALEX) and two diode lasers: OBIS 532-100-LS (Coherent, USA), operated at 60 µW for donor molecules at 532 nm, and OBIS 640-100-LX (Coherent, USA), operated at 25 µW for acceptor molecules at 640 nm, both in alternation mode with a 100 µs period. The lasers were combined by an aspheric fiber port (PAF2S-11A, Thorlabs, USA), coupled into a polarization-maintaining single-mode fiber P3-57 488PM-FC-2 (Thorlabs, USA) and collimated (RC12APC-P01, Thorlabs, USA) before entering an epi-illuminated confocal microscope (Olympus IX71, Hamburg, Germany). Excitation and emission collection was done by the same water immersion objective (60X, NA 1.2, UPlanSAPO 60XO, Olympus, Japan) and spectral separation was achieved by a dual-edge beamsplitter ZT532/640rpc (Chroma/AHF, Germany). Fluorescence emitted from the sample was collected by the same objective and further focused via an achromatic lens (AC254-200-A, Thorlabs) directly into the single-photon avalanche diodes (PDM 50-Micron, MPD). The small active area of the detectors (ø 50 µm) served as a pinhole. Before that, the photon streams were spectrally split into the donor and acceptor channels by a single-edge dichroic mirror H643 LPXR (AHF, Germany). Fluorescence emission was filtered by band-pass filters directly in front of each detector: for the donor channel FF01-582/75-25 (Semrock/AHF, Germany) and ET700/75m Chroma (AHF, Germany) for the acceptor channel. The detector outputs were recorded by an NI-Card PCI-6602 (National Instruments, USA) using LabView data acquisition software from the Weiss laboratory[61]. Auto-alignment utilized a counter/timer device module (USB-CTR04, Measurement Computing, USA) with custom-made acquisition software written in Python, available at https://github.com/klockeph/mcc-daq-acquisition.

Data analysis was performed using a home-written software package, as described previously [60]. Single bursts were identified first using All-Photon-Burst-Search (APBS) with a threshold for burst start/stop of 15 photons[35], a time window of 500 µs, and a minimum total photon number of 150 within the burst. Based on these data donor leakage (α) and direct acceptor excitation (δ) were determined as mean values from a 1D-fit of background-corrected donor-only E* and acceptor-only S* distributions. Then, a Dual-Channel-Burst-Search (DCBS) was performed with similar parameters to determine excitation flux (β) and detection efficiency and quantum yields (γ)[37]. E-histograms of double-labelled FRET species were generally extracted by selecting 0.3 < S

bioRxiv preprint doi: https://doi.org/10.1101/2023.12.29.573596; this version posted December 29, 2023. The copyright holder for this preprint (which was not certified by peer review) is the author/funder, who has granted bioRxiv a license to display the preprint in perpetuity. It is made available under aCC-BY-NC 4.0 International license.

< 0.7. E-histograms were fitted with a Gaussian function according to $\frac{1}{\sigma\sqrt{2\pi}}e^{-\frac{(E-\mu)^2}{2\sigma^2}}$, where *E* represents the measured FRET efficiency for every detected molecule, μ is the mean, and σ the standard deviation.

For FRET efficiency to inter-dye distance conversion, the Förster equation was used:

$$R_{DA} = R_0\sqrt[6]{(1-E)/E} \qquad \textbf{eqn. 3}$$

The Förster radius R_0 is given by the following equation[62]:

$$R_0^6 = \frac{9\ln(10)}{128\pi^5 N_A}\frac{\kappa^2}{n^4}Q_D\frac{\int_0^\infty F_D(\lambda)\varepsilon_A(\lambda)\lambda^4 d\lambda}{\int_0^\infty F_D(\lambda)d\lambda} \qquad \textbf{eqn. 4}$$

where N_A is the Avogadro constant, κ^2 the dipole orientation factor, n the averaged refractive index of the medium, Q_D the donor quantum yield, F_D the donor emission spectrum, and the acceptor absorbance spectrum ε_A. We used values of R_0 known from the literature: Cy3-ATTO647N: R_0 = 5.1 nm[51,52]; Cy3B-ATTO647N: R_0 = 6.7 nm[52–54]. For Cy3B-Cy5 we used an unpublished approach to determine R_0 = 7.4 nm by least-square fitting of the data (E values) to the known inter-dye distances of donor and acceptor on the dsDNA[53] using equation 3.

μEpi. The setup for widefield imaging utilizes an external fiber-coupled laser box (READY BeamTM ind 2 1007773, Fisba, Lithuania). A 640 nm wavelength continuous-wave excitation laser was used which provides an output of 30 mW (measured after the objective). The beam was collimated through a parabolic mirror (RC04APC-P01, Thorlabs), passes through a clean-up filter (ZET 635/10 ⌀25 mm, Chroma), and was expanded with a plano-concave lens (f = -25 mm, LC1054-ML - Ø1/2, Thorlabs). A plano-convex lens (f = 60 mm, LA1134-A-ML - Ø1, Thorlabs) focuses the beam into the back focal plane of the objective. A dichroic beam splitter with high reflectivity at 640 nm (ZT532/640rpc, Chroma, USA) separates excitation and emission beams into and from a high numerical aperture (NA) apo-chromatic oil immersion objective (60X, NA 1.35, UPLSAPO60XO, Olympus, Japan). Fluorescence emitted from the sample was collected by the same objective and was further focused via an achromatic lens (AC254-150-A-ML, Thorlabs), projecting a real image onto the chip of a CMOS camera (U3-30C0CP-M-GL rev.2.2, IDS)[63]. The photon stream is further filtered with a band-pass filter (ET700/75m Chroma, AHF, Germany) before reaching the camera sensor.

The photoswitching of the fluorophores was achieved by adding 500 µl of an oxygen scavenging system buffer [58] (pyranose oxidase at 3 U/mL, catalase at a final concentration of 90 U/mL, and 40 mM glucose in PBS) mixed with 0.1% (v/v) ß-mercaptoethanol. The laser power used for imaging was 30 mW, which corresponds to approximately 0.1 kW/cm^2 with an illuminated area of 140 x 140 µm^2. Diffraction limited recordings were acquired using the original software that came with the cameras. All recordings were done at 10 frames per second, with an exposure time of 100 ms and the analog gain set at maximum.

Super-resolution image reconstruction was performed using the ImageJ plug-in Thunderstorm[56]. Each localization was filtered using a B-Spline wavelet filter as described. The local maxima method was employed for the approximate localization of the molecules. Sub-pixel localization was achieved by fitting an Integrated Gaussian model using a weighted least squares method with a 3-pixel fitting radius. The super-resolution image was rendered with a pixel size of 12 x 12 nm^2. For STORM, drift correction was implemented using the fiducial marker algorithm with fluorescent tetraspeck beads (100 nm, Thermo Fisher) on the sample. The maximal search tracking distance was set at 20 nm, and the minimum visibility ratio was maintained at 0.9 per frame. For PAINT,

bioRxiv preprint doi: https://doi.org/10.1101/2023.12.29.573596; this version posted December 29, 2023. The copyright holder for this preprint (which was not certified by peer review) is the author/funder, who has granted bioRxiv a license to display the preprint in perpetuity. It is made available under aCC-BY-NC 4.0 International license.

drift correction was performed using a cross-correlation algorithm, correlating the positioning of all blinking events of each molecule in the movie over time.

Online Methods References

58. Zhang, L. *et al.* Linker Molecules Convert Commercial Fluorophores into Tailored Functional Probes during Biolabelling. *Angew Chem Int Ed Engl* **61**, e202112959 (2022).

59. de Boer, M. *et al.* Conformational and dynamic plasticity in substrate-binding proteins underlies selective transport in ABC importers. *eLife* **8**, e44652 (2019).

60. Gouridis, G. *et al.* Conformational dynamics in substrate-binding domains influences transport in the ABC importer GlnPQ. *Nat Struct Mol Biol* **22**, 57–64 (2015).

61. Ingargiola, A. *et al.* Multispot single-molecule FRET: High-throughput analysis of freely diffusing molecules. *PLOS ONE* **12**, e0175766 (2017).

62. Förster, Th. Zwischenmolekulare Energiewanderung und Fluoreszenz. *Annalen der Physik* **437**, 55–75 (1948).

63. Diekmann, R. *et al.* Characterization of an industry-grade CMOS camera well suited for single molecule localization microscopy – high performance super-resolution at low cost. *Sci Rep* **7**, 14425 (2017).

bioRxiv preprint doi: https://doi.org/10.1101/2023.12.29.573596; this version posted December 29, 2023. The copyright holder for this preprint (which was not certified by peer review) is the author/funder, who has granted bioRxiv a license to display the preprint in perpetuity. It is made available under aCC-BY-NC 4.0 International license.

Supplementary Information for the article

Single-molecule detection and super-resolution imaging with a portable and adaptable 3D-printed microscopy platform (Brick-MIC)

Gabriel G. Moya Muñoz[1,+], Oliver Brix[1,+], Philipp Klocke[1], Nicolas D. Wendler[1], Eitan Lerner[2,3], Niels Zijstra[1], Thorben Cordes[1,*]

[1]Physical and Synthetic Biology, Faculty of Biology, Ludwig-Maximilians Universität München, Planegg-Martinsried, Germany
[2]Department of Biological Chemistry, The Alexander Silberman Institute of Life Sciences, Faculty of Mathematics Science, The Edmond J.Safra Campus, The Hebrew University of Jerusalem, Jerusalem 9190401, Israel
[3]The Center for Nanoscience and Nanotechnology, The Hebrew University of Jerusalem, Jerusalem 9190401, Israel

*corresponding author: cordes@bio.lmu.de
[+]these authors contributed equally to this work

bioRxiv preprint doi: https://doi.org/10.1101/2023.12.29.573596; this version posted December 29, 2023. The copyright holder for this preprint (which was not certified by peer review) is the author/funder, who has granted bioRxiv a license to display the preprint in perpetuity. It is made available under aCC-BY-NC 4.0 International license.

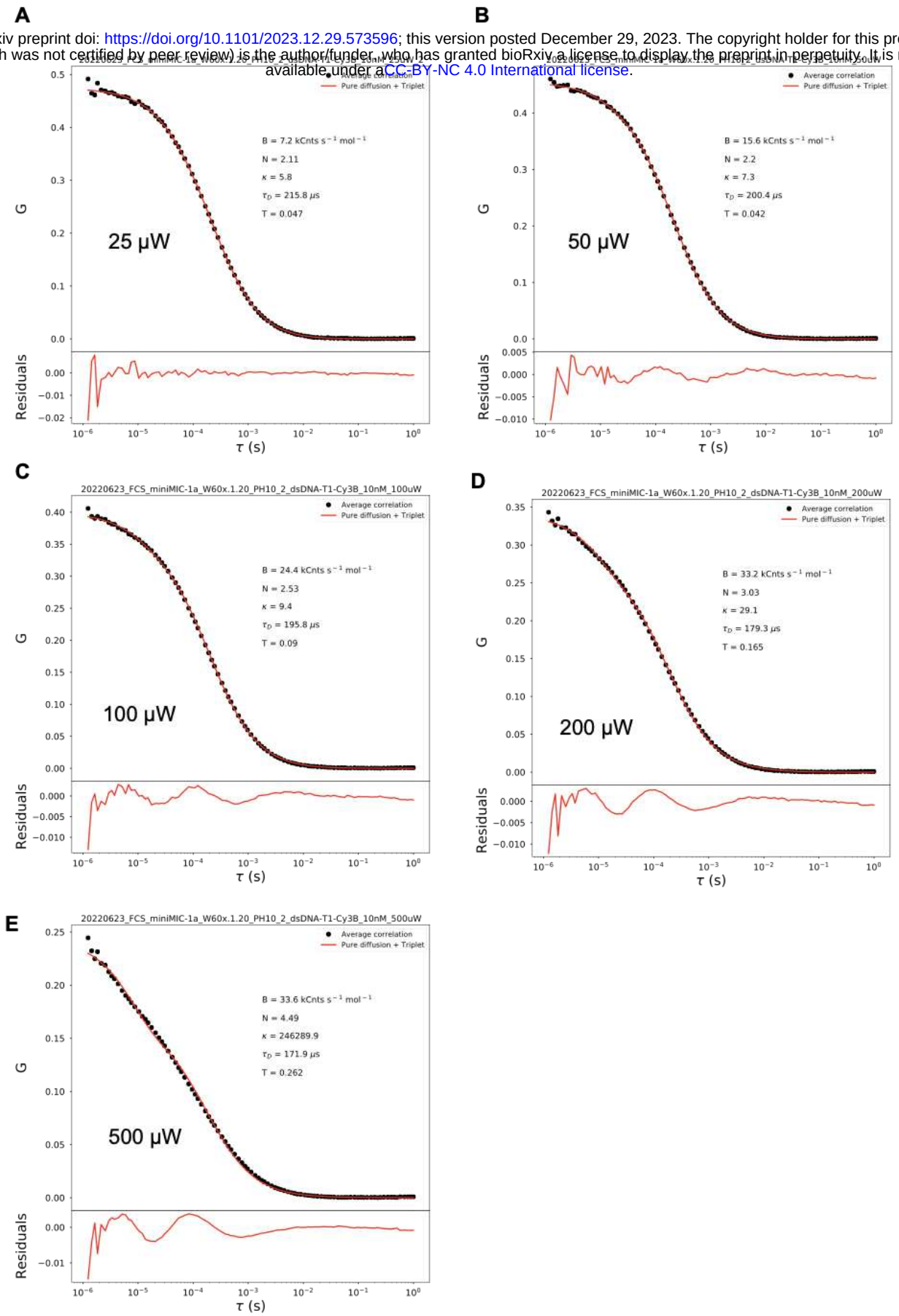

Supplementary Figure 1: FCS laser power dependency of a 10 nM solution of a 40mer dsDNA sample labelled with Cy3B with the use of 10 µm Pinhole.

bioRxiv preprint doi: https://doi.org/10.1101/2023.12.29.573596; this version posted December 29, 2023. The copyright holder for this preprint (which was not certified by peer review) is the author/funder, who has granted bioRxiv a license to display the preprint in perpetuity. It is made available under aCC-BY-NC 4.0 International license.

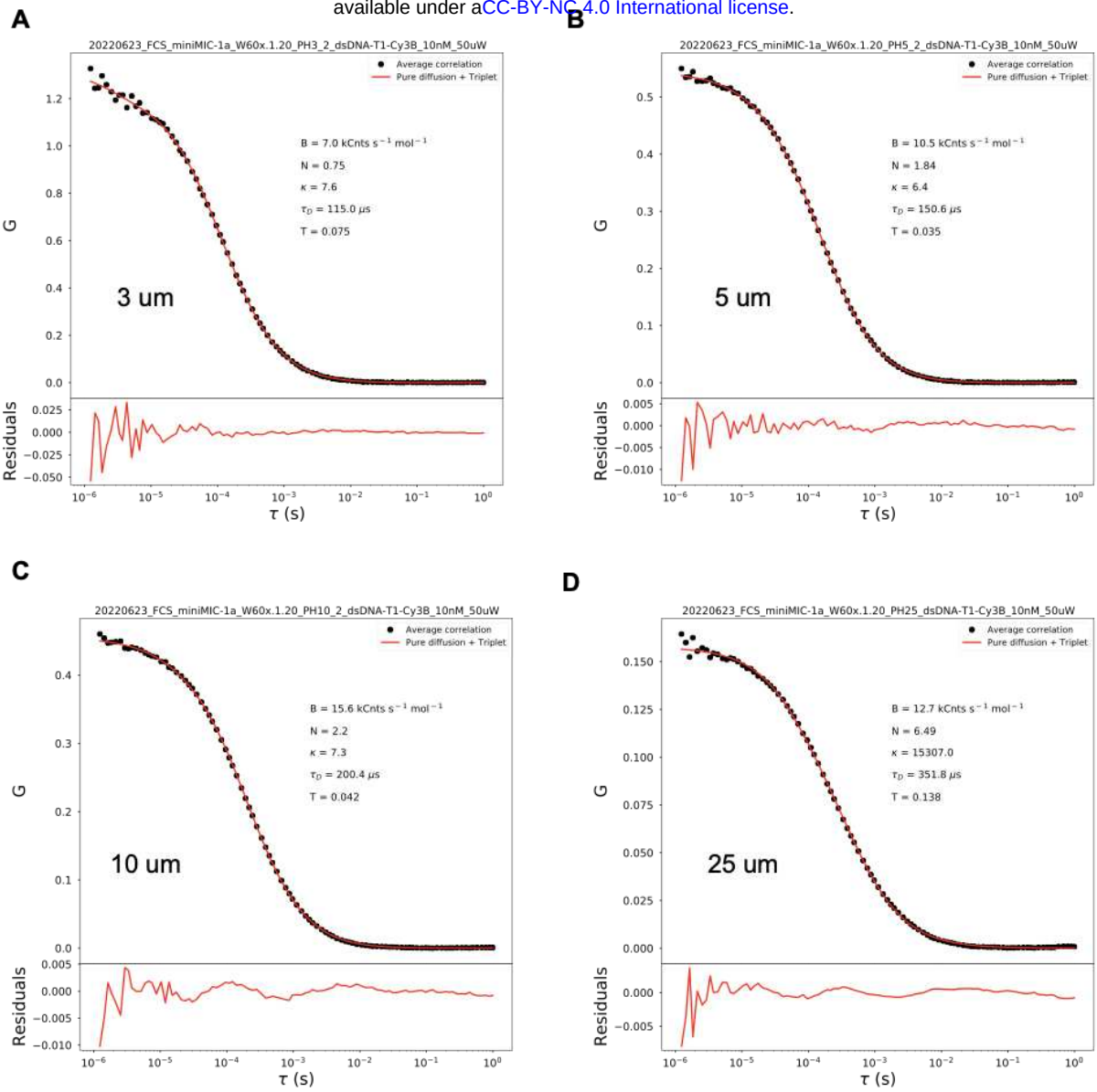

Supplementary Figure 2: FCS Pinhole size dependency of a 10 nM solution of a 40mer dsDNA sample labelled with Cy3B and excited at 50 µW laser power.

bioRxiv preprint doi: https://doi.org/10.1101/2023.12.29.573596; this version posted December 29, 2023. The copyright holder for this preprint (which was not certified by peer review) is the author/funder, who has granted bioRxiv a license to display the preprint in perpetuity. It is made available under aCC-BY-NC 4.0 International license.

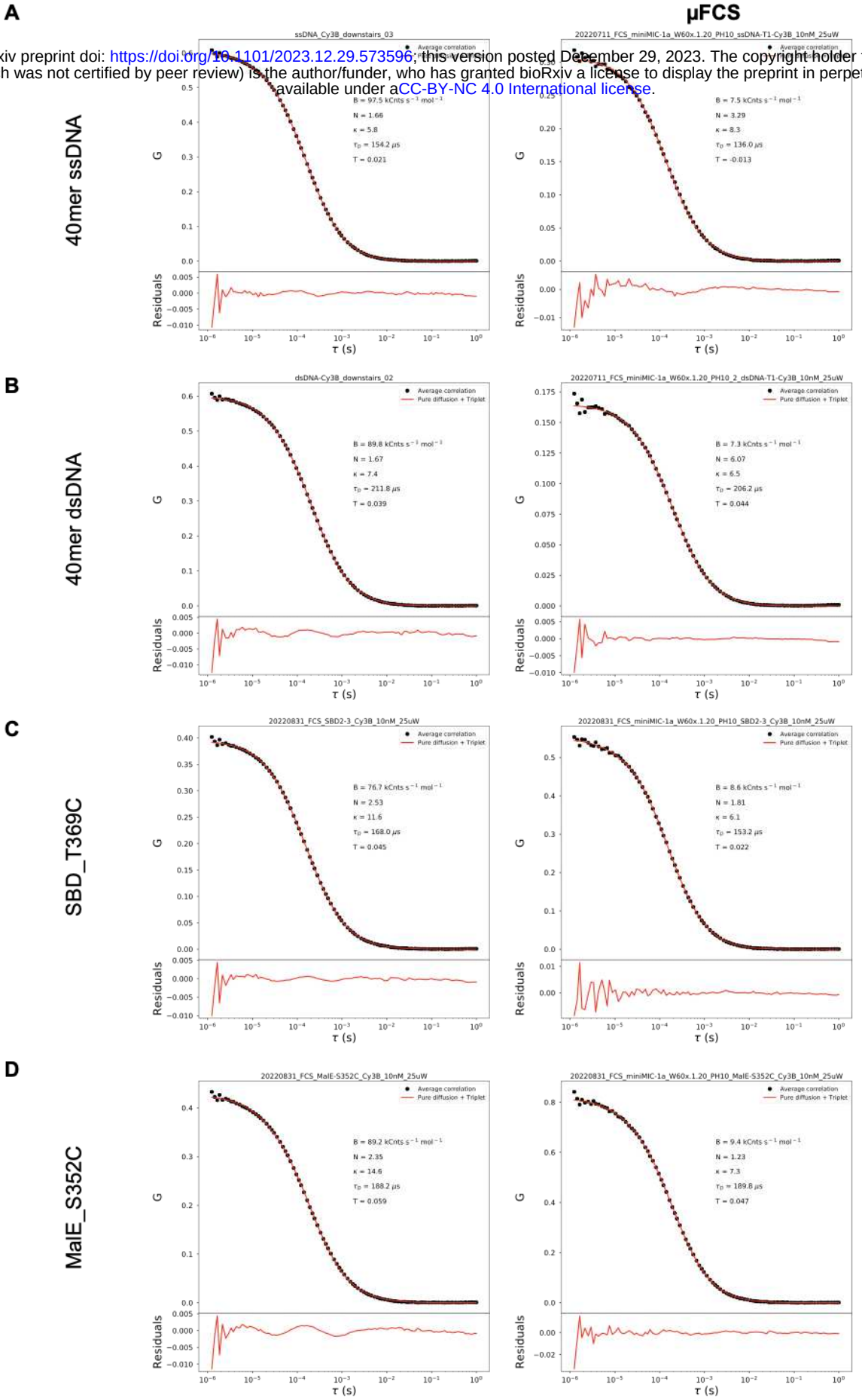

Supplementary Figure 3: FCS comparison between Brick-Mic (10 µm Pinhole) and the lab's confocal setup using various biomolecules with different masses and hydrodynamic radii at a 25 µW laser power.

bioRxiv preprint doi: https://doi.org/10.1101/2023.12.29.573596; this version posted December 29, 2023. The copyright holder for this preprint (which was not certified by peer review) is the author/funder, who has granted bioRxiv a license to display the preprint in perpetuity. It is made available under aCC-BY-NC 4.0 International license.

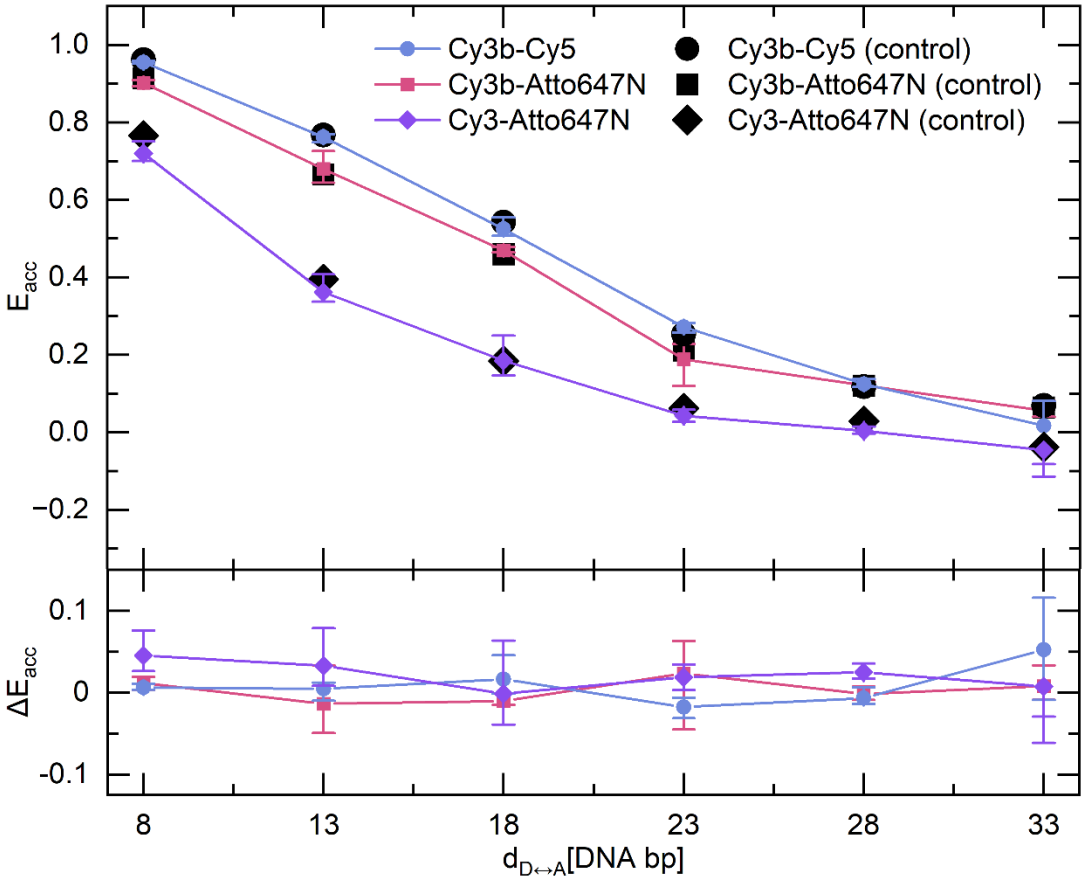

Supplementary Figure 4: Accurate FRET values comparison between Brick-MIC and a standard conocal microscope. smFRET measurements were performed on donor and acceptor fluorophore pairs Cy3B-Cy5, C3b-Atto647N and Cy3-Atto647n which were covalently labelled to dsDNA (with distances between donor and acceptor fluorophore pairs in terms of DNA base pairs 8, 13, 18, 23, 28 and 33). Setup independent accurate FRET values were compared between the BRICK-MIC ALEX modality (coloured symbols) and our standard confocal microscope (black filled symbols).

bioRxiv preprint doi: https://doi.org/10.1101/2023.12.29.573596; this version posted December 29, 2023. The copyright holder for this preprint (which was not certified by peer review) is the author/funder, who has granted bioRxiv a license to display the preprint in perpetuity. It is made available under aCC-BY-NC 4.0 International license.

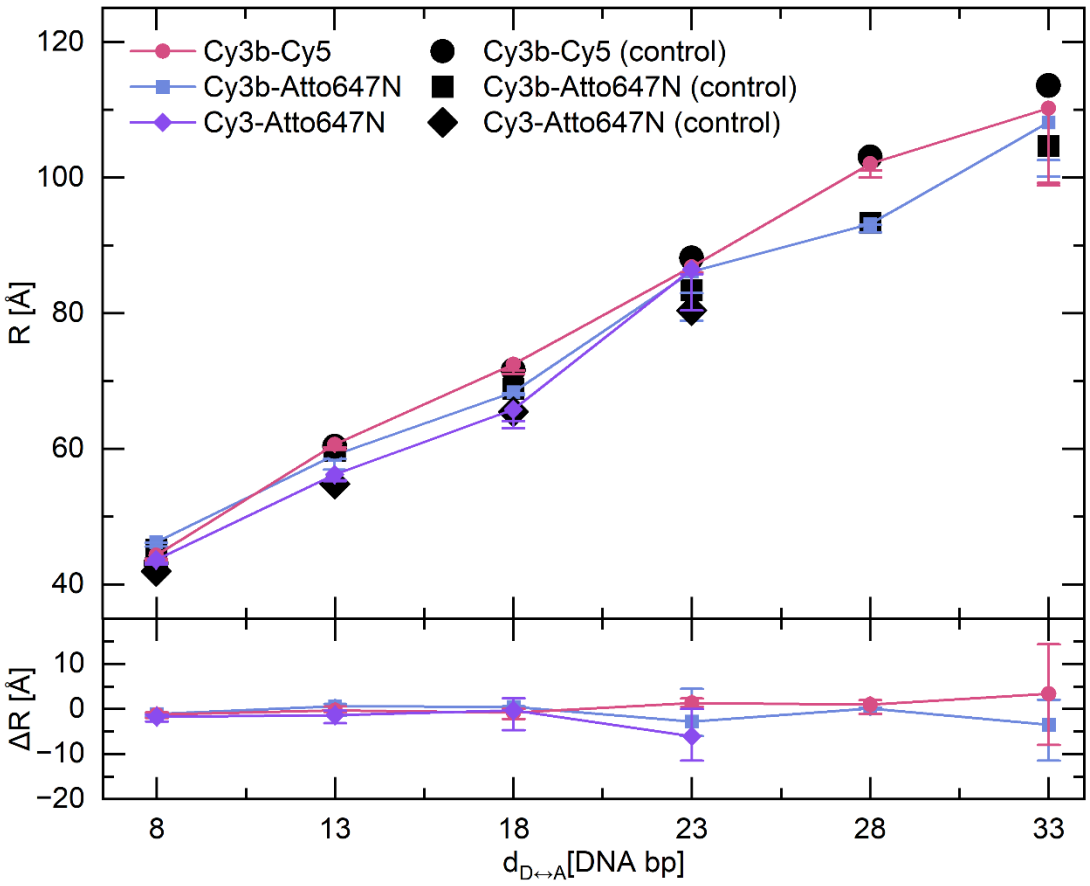

Supplementary Figure 5: Calculated distances comparison between BRICK-MIC and standard confocal microscope. The setup independent accurate FRET values were used to calculate the distances in Å between donor and acceptor fluorophore pairs (i. e. Cy3B-Cy5, Cy3B-Atto647N and Cy3-Atto647N) subjected to the DNA base pair distances 8, 13, 18, 23, 28 and 33. Filled coloured symbols display smFRET measurements performed on the BRICK-MIC and black filled symbols display measurements on our standard confocal microscope.

bioRxiv preprint doi: https://doi.org/10.1101/2023.12.29.573596; this version posted December 29, 2023. The copyright holder for this preprint (which was not certified by peer review) is the author/funder, who has granted bioRxiv a license to display the preprint in perpetuity. It is made available under aCC-BY-NC 4.0 International license.

Supplementary Table 1: Summary of smFRET fit results obtained with Brick-Mic for the Cy3B and Atto647N DNA ladder through fitting with a 2D Gaussian model.

bp	8	13	18	23	28	33
E*	0.84	0.58	0.35	0.20	0.15	0.12
σ_{E^*}	0.06	0.09	0.07	0.05	0.04	0.04
S*	0.54	0.57	0.64	0.66	0.69	0.69
σ_{S^*}	0.07	0.07	0.07	0.06	0.06	0.06

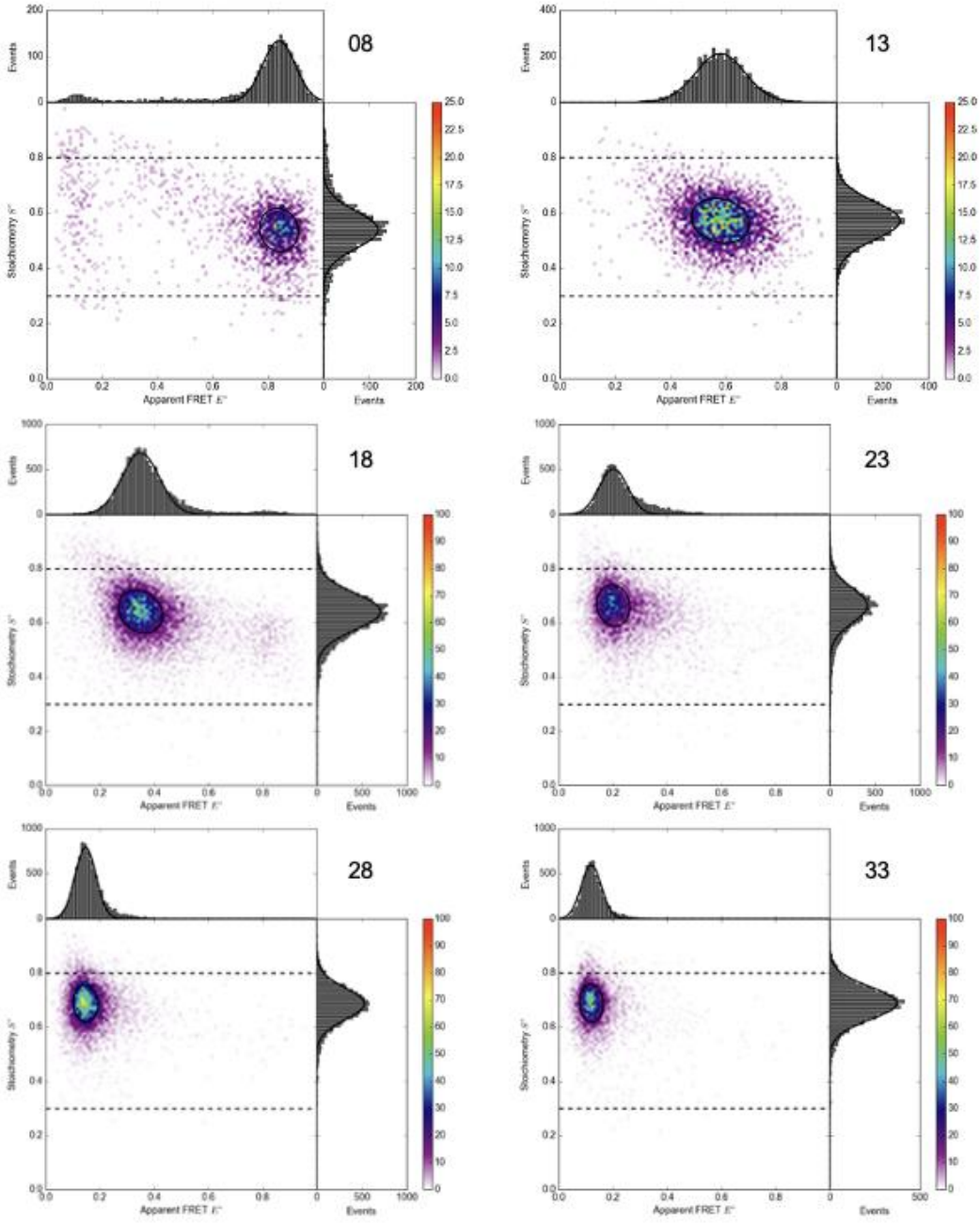

Supplementary Figure 6: Uncorrected ES-histograms (apparent FRET) obtained with Brick-Mic corresponding to a DNA ladder labeled with Cy3B and Atto647N. The corresponding distances are 8 bp (top-left), 13 bp (top-right), 18 bp (middle-left), 23 bp (middle-right), 28 bp (lower-left) and 33 bp (lower-right).

bioRxiv preprint doi: https://doi.org/10.1101/2023.12.29.573596; this version posted December 29, 2023. The copyright holder for this preprint (which was not certified by peer review) is the author/funder, who has granted bioRxiv a license to display the preprint in perpetuity. It is made available under aCC-BY-NC 4.0 International license.

Supplementary Table 2: Summary of smFRET fit results obtained with Brick-Mic for the Cy3B and Cy5 DNA ladder through fitting with a 2D Gaussian model.

bp	8	13	18	23	28	33
E^*	0.87	0.56	0.33	0.19	0.13	0.13
σ_{E^*}	0.06	0.10	0.07	0.05	0.04	0.03
S^*	0.59	0.64	0.73	0.76	0.81	0.79
σ_{S^*}	0.06	0.07	0.07	0.06	0.05	0.05

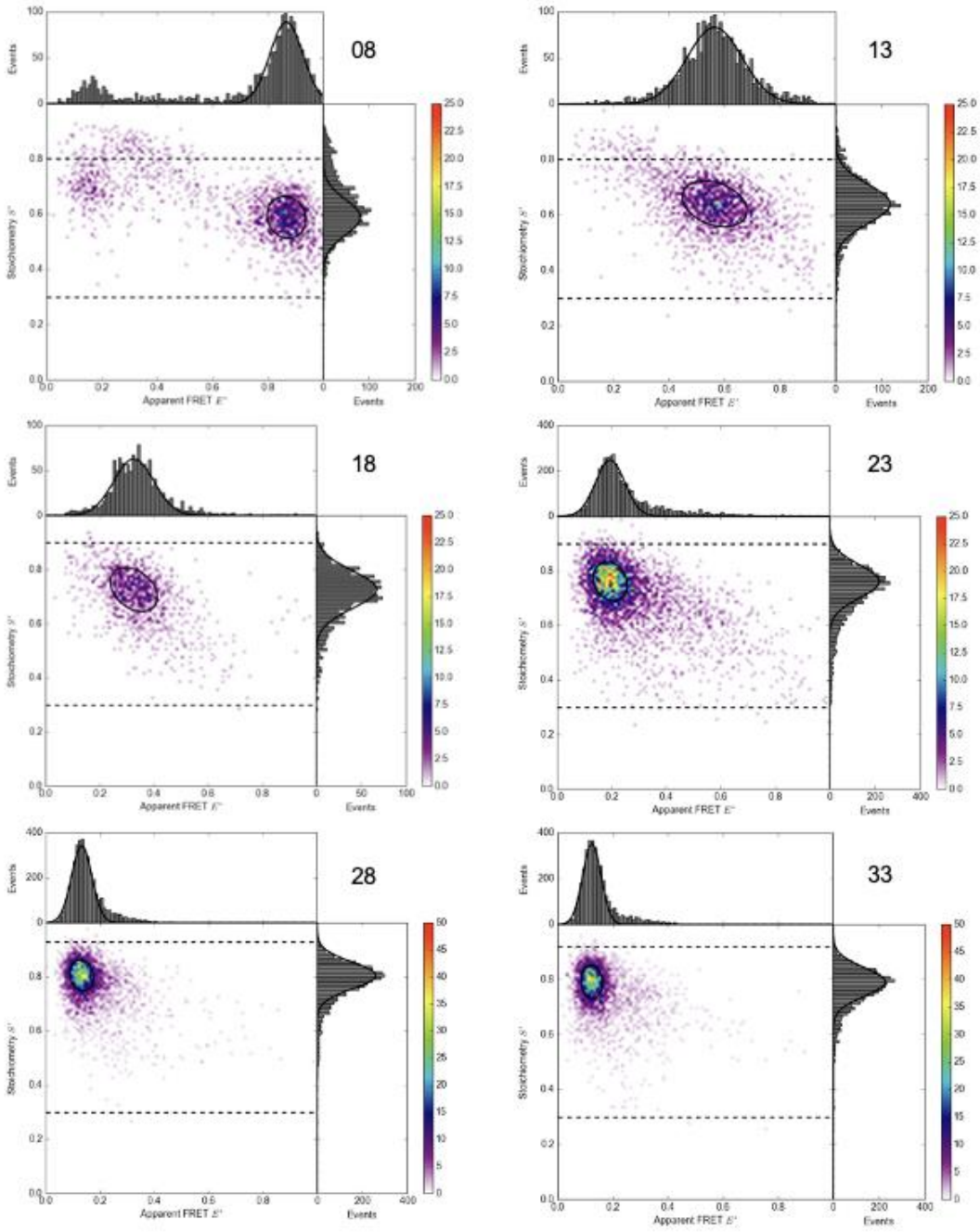

Supplementary Figure 7: Uncorrected ES-histograms (apparent FRET) obtained with Brick-Mic corresponding to a DNA ladder labelled with Cy3B and Cy5. The corresponding distances are 8 bp (top-left), 13 bp (top-right), 18 bp (middle-left), 23 bp (middle-right), 28 bp (lower-left) and 33 bp (lower-right).

bioRxiv preprint doi: https://doi.org/10.1101/2023.12.29.573596; this version posted December 29, 2023. The copyright holder for this preprint (which was not certified by peer review) is the author/funder, who has granted bioRxiv a license to display the preprint in perpetuity. It is made available under aCC-BY-NC 4.0 International license.

Supplementary Table 3: Summary of smFRET fit results obtained with Brick-MIC for the Cy3 and Atto647N DNA ladder through fitting with a 2D Gaussian model.

bp	8	13	18	23	28	33
E^*	0.84	0.58	0.36	0.21	0.17	0.14
σ_{E^*}	0.06	0.08	0.08	0.07	0.06	0.05
S^*	0.50	0.44	0.42	0.42	0.41	0.40
σ_{S^*}	0.06	0.06	0.06	0.06	0.07	0.07

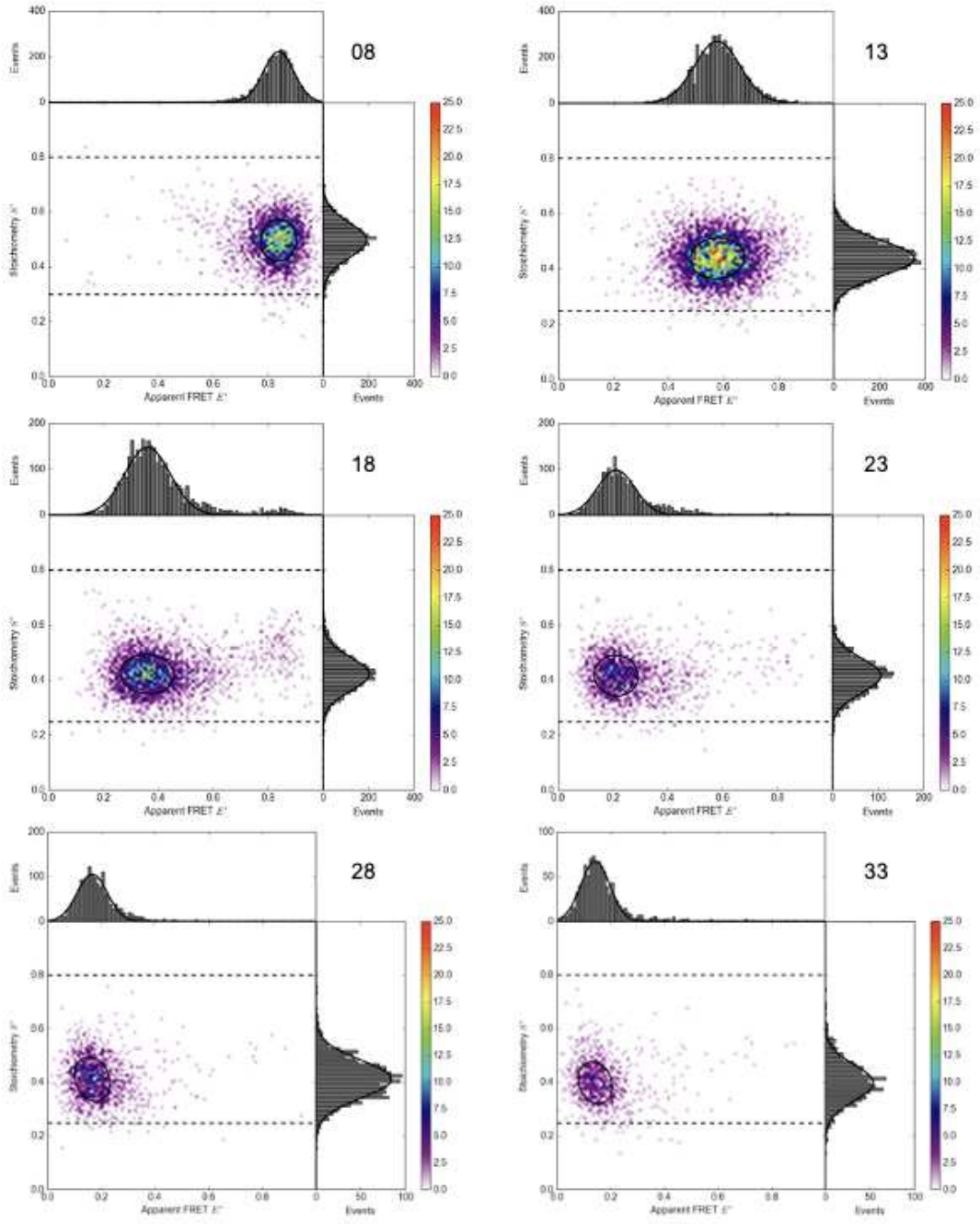

Supplementary Figure 8: Uncorrected ES-histograms (apparent FRET) obtained with Brick-Mic corresponding to a DNA ladder labelled with Cy3 and Atto647N. The corresponding distances are 8 bp (top-left), 13 bp (top-right), 18 bp (middle-left), 23 bp (middle-right), 28 bp (lower-left) and 33 bp (lower-right).

bioRxiv preprint doi: https://doi.org/10.1101/2023.12.29.573596; this version posted December 29, 2023. The copyright holder for this preprint (which was not certified by peer review) is the author/funder, who has granted bioRxiv a license to display the preprint in perpetuity. It is made available under aCC-BY-NC 4.0 International license.

Supplementary Table 4: Summary of smFRET fit results obtained with the lab's ALEX microscope for the Cy3B and Atto647N DNA ladder through fitting with a 2D Gaussian model.

bp	8	13	18	23	28	33
E^*	0.90	0.65	0.47	0.28	0.22	0.19
σ_{E^*}	0.04	0.08	0.07	0.05	0.04	0.04
S^*	0.53	0.55	0.58	0.58	0.59	0.59
σ_{S^*}	0.06	0.07	0.08	0.07	0.07	0.07

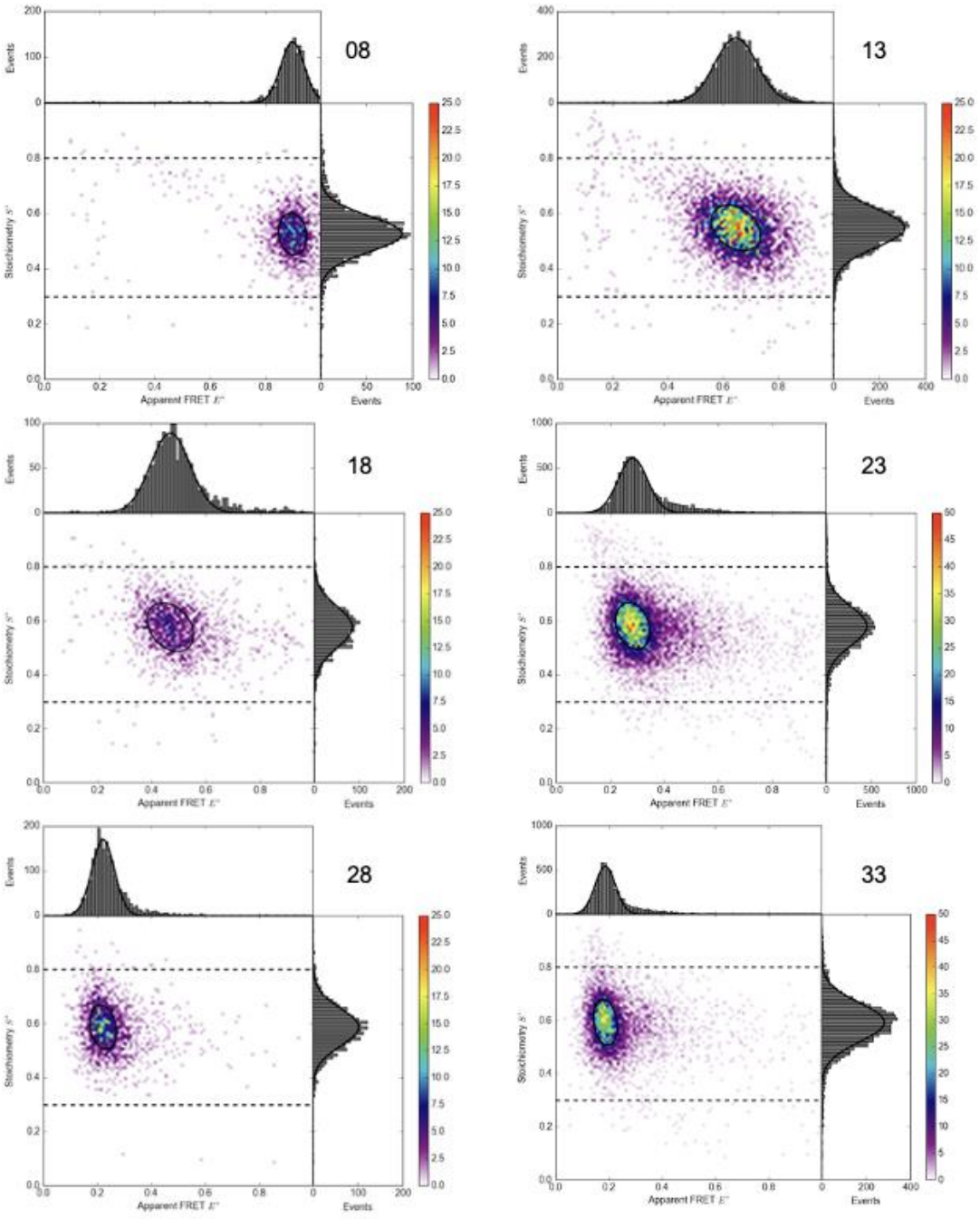

Supplementary Figure 9: Uncorrected ES-histograms (apparent FRET) obtained with the lab's ALEX microscope corresponding to a DNA ladder labelled with Cy3B and Atto647N. The corresponding distances are 8 bp (top-left), 13 bp (top-right), 18 bp (middle-left), 23 bp (middle-right), 28 bp (lower-left) and 33 bp (lower-right).

bioRxiv preprint doi: https://doi.org/10.1101/2023.12.29.573596; this version posted December 29, 2023. The copyright holder for this preprint (which was not certified by peer review) is the author/funder, who has granted bioRxiv a license to display the preprint in perpetuity. It is made available under a CC-BY-NC 4.0 International license.

Supplementary Table 5: Summary of smFRET fit results obtained with the lab's ALEX microscope for the Cy3 and Atto647N DNA ladder through fitting with a 2D Gaussian model.

bp	8	13	18	23	28	33
E*	0.91	0.70	0.50	0.32	0.27	0.23
σ_{E^*}	0.04	0.08	0.09	0.08	0.07	0.06
S*	0.46	0.38	0.33	0.30	0.29	0.29
σ_{S^*}	0.07	0.06	0.06	0.06	0.06	0.06

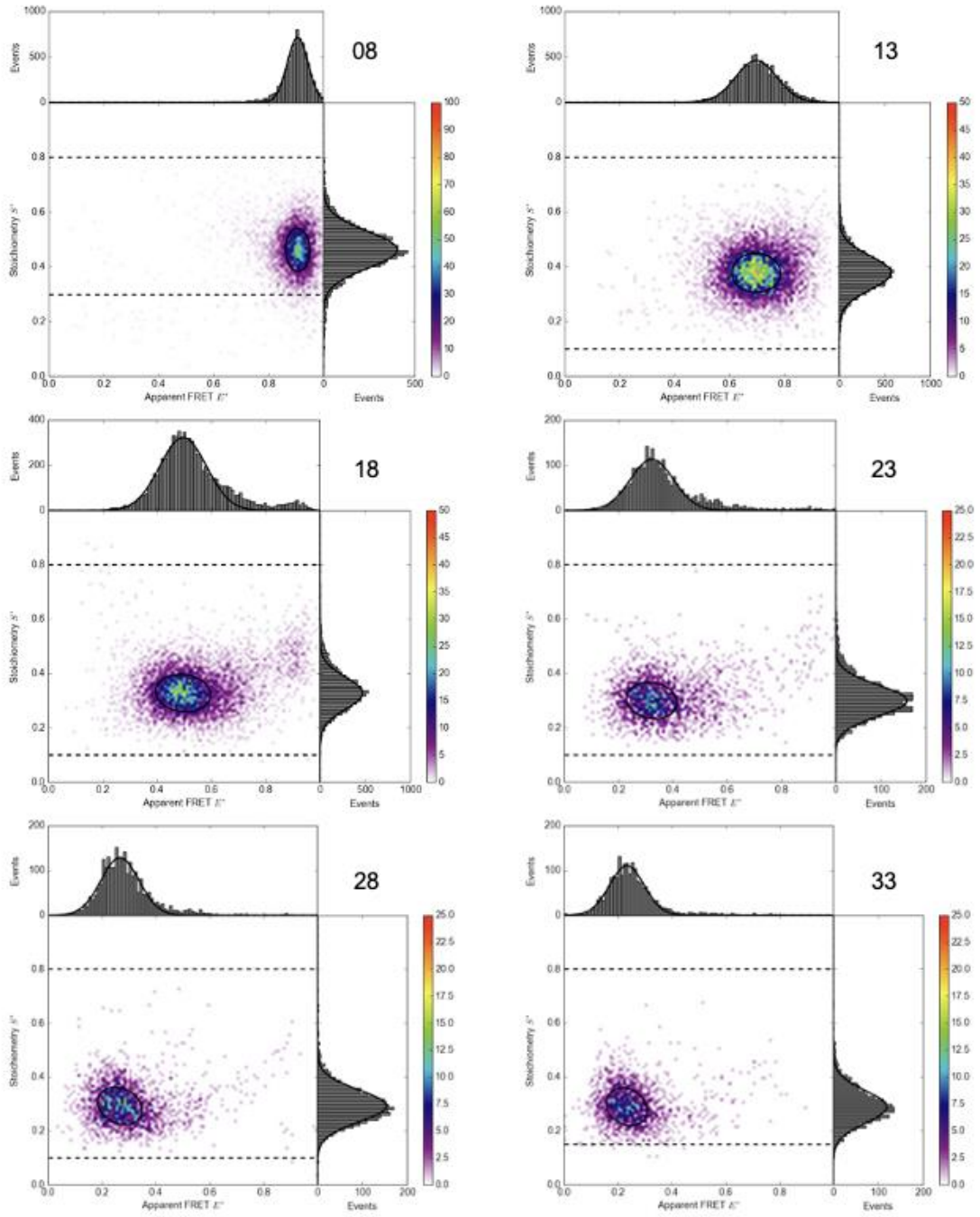

Supplementary Figure 10: Uncorrected ES-histograms (apparent FRET) obtained with the lab's ALEX microscope corresponding to a DNA ladder labelled with Cy3 and Atto647N. The corresponding distances are 8 bp (top-left), 13 bp (top-right), 18 bp (middle-left), 23 bp (middle-right), 28 bp (lower-left) and 33 bp (lower-right).

bioRxiv preprint doi: https://doi.org/10.1101/2023.12.29.573596; this version posted December 29, 2023. The copyright holder for this preprint (which was not certified by peer review) is the author/funder, who has granted bioRxiv a license to display the preprint in perpetuity. It is made available under aCC-BY-NC 4.0 International license.

Supplementary Table 6: Summary of smFRET fit results obtained with the lab's ALEX microscope for the Cy3B and Cy5 DNA ladder through fitting with a 2D Gaussian model.

bp	8	13	18	23	28	33
E*	0.93	0.67	0.46	0.27	0.20	0.18
σ_{E^*}	0.04	0.09	0.07	0.06	0.04	0.04
S*	0.55	0.57	0.62	0.69	0.70	0.70
σ_{S^*}	0.08	0.08	0.08	0.07	0.07	0.07

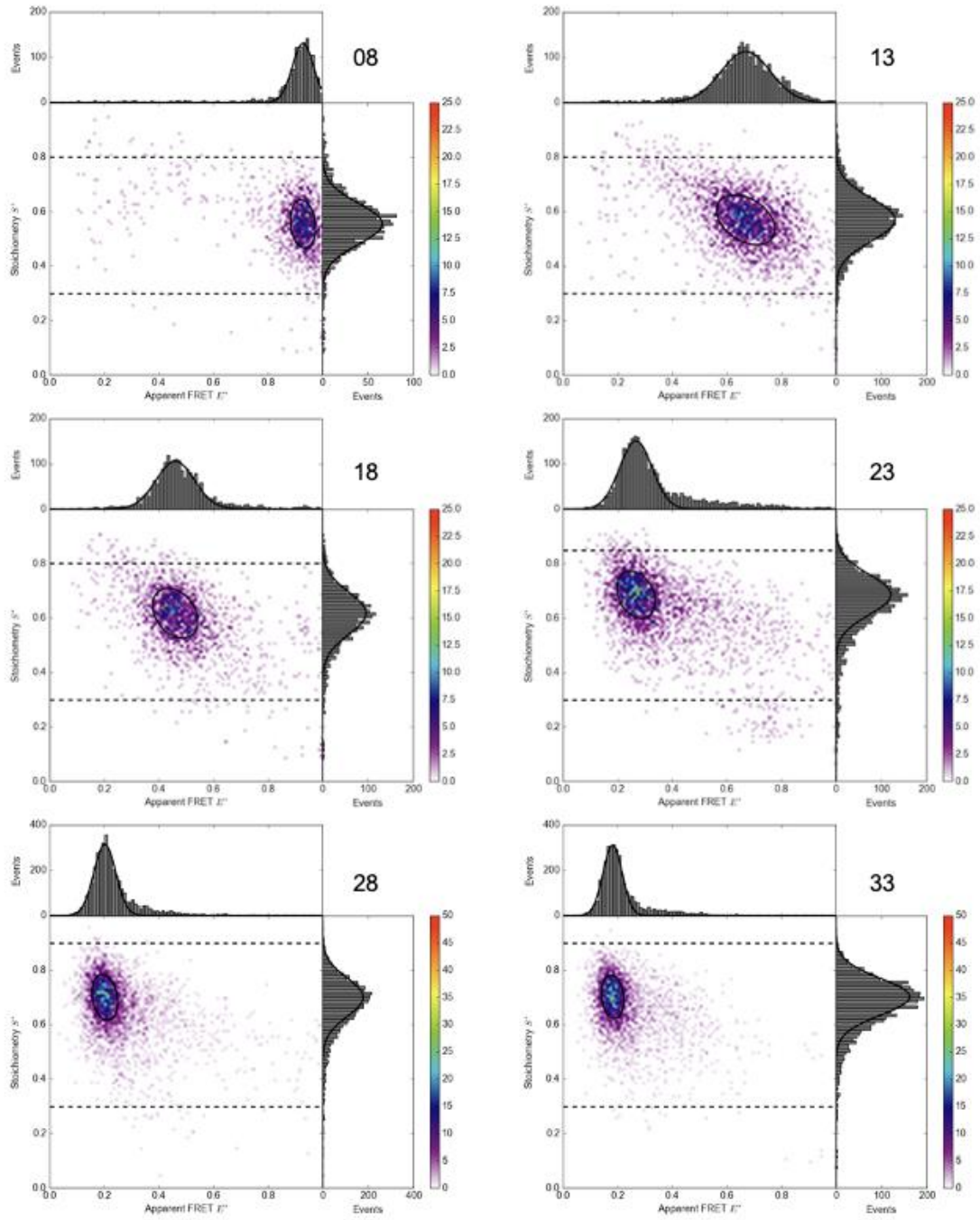

Supplementary Figure 11: Uncorrected ES-histograms (apparent FRET) obtained with the lab's ALEX microscope corresponding to a DNA ladder labelled with Cy3B and Cy5. The corresponding distances are 8 bp (top-left), 13 bp (top-right), 18 bp (middle-left), 23 bp (middle-right), 28 bp (lower-left) and 33 bp (lower-right).

bioRxiv preprint doi: https://doi.org/10.1101/2023.12.29.573596; this version posted December 29, 2023. The copyright holder for this preprint (which was not certified by peer review) is the author/funder, who has granted bioRxiv a license to display the preprint in perpetuity. It is made available under aCC-BY-NC 4.0 International license.

Supplementary Table 7: Accurate FRET analysis of DNA Cy3B-Atto647N measured with Brick-MIC. Correction factors for leakage α, direct excitation δ, detection corrections β and γ and accurate FRET values and calculated distance.

bp	8		13		18		23		28		33	
α	0.081		0.088		0.082		0.082		0.081		0.083	
+/- Δ_α	0.004	0.004	0.01	0.02	0.006	0.005	0.001	0.001	0.006	0.005	0.005	0.007
δ	0.038		0.041		0.044		0.044		0.046		0.045	
+/- Δ_δ	0.004	0.008	0.002	0.003	0.004	0.002	0.002	0.004	0.002	0.002	0.002	0.003
β	1.00											
+/- Δ_β	0.050						0.03					
γ	0.51											
+/- Δ_γ	0.11						0.07					
$S_{accMean}$	0.495		0.503		0.515		0.54		0.498		0.48	
+/- Δ_{Sacc} -	0.003	0.003	0.015	0.008	0.014	0.011	0.09	0.05	0.002	0.003	0.02	0.02
$E_{accMean}$	0.902		0.68		0.470		0.19		0.122		0.06	
+/- Δ_{Eacc}	0.007	0.009	0.05	0.04	0.009	0.005	0.04	0.07	0.009	0.008	0.03	0.02
R [Å]	46.3		59.1		68.4		86		93.2		108	
+/- Δ_R [Å]	0.1	0.7	0.5	2.2	0.2	0.4	7	3	0.2	1.3	6	8

bioRxiv preprint doi: https://doi.org/10.1101/2023.12.29.573596; this version posted December 29, 2023. The copyright holder for this preprint (which was not certified by peer review) is the author/funder, who has granted bioRxiv a license to display the preprint in perpetuity. It is made available under a CC-BY-NC 4.0 International license.

Supplementary Table 8: Accurate FRET analysis of DNA Cy3B-Cy5 measured with Brick-MIC. Correction factors for leakage α, direct excitation δ, detection corrections β and γ and accurate FRET and calculated distance values.

bp	**8**		**13**		**18**		**23**		**28**		**33**	
α	0.075		0.077		0.073		0.078		0.073		0.073	
+/- Δ_α	0.002	0.002	0.005	0.004	0.001	0.002	0.006	0.004	0.0010	0.0010	0.007	0.006
δ	0.05		0.05		0.081		0.079		0.087		0.079	
+/- Δ_δ	0.04	0.05	0.03	0.05	0.007	0.012	0.012	0.014	0.004	0.003	0.004	0.003
β	0.90											
+/- Δ_β	0.07						0.04					
γ	0.32											
+/- Δ_γ	0.06						0.08					
$S_{accMean}$	0.50		0.49		0.50		0.51		0.53		0.53	
+/- Δ_{Sacc} -	0.01	0.01	0.01	0.01	0.01	0.02	0.02	0.02	0.01	0.02	0.01	0.01
$E_{accMean}$	0.955		0.763		0.53		0.272		0.124		0.02	
+/- Δ_{Eacc}	0.005	0.003	0.007	0.014	0.03	0.02	0.011	0.014	0.014	0.007	0.06	0.06
R [Å]	44.3		60.7		72.5		86.9		102		110	
+/- Δ_R [Å]	0.5	0.8	0.8	0.4	0.9	1.4	1.0	0.8	1	2	11	11

bioRxiv preprint doi: https://doi.org/10.1101/2023.12.29.573596; this version posted December 29, 2023. The copyright holder for this preprint (which was not certified by peer review) is the author/funder, who has granted bioRxiv a license to display the preprint in perpetuity. It is made available under aCC-BY-NC-4.0 International license.

Supplementary Table 9: Accurate FRET analysis of DNA Cy3-Atto647N measured on with Brick-MIC. Correction factors for leakage α, direct excitation δ, detection corrections β and γ and accurate FRET values and calculated distance.

bp	**8**		**13**		**18**		**23**		**28**		**33**	
α	0.054		0.064		0.071		0.063		0.05		0.055	
+/- Δ_α	0.007	0.009	0.006	0.005	0.011	0.009	0.004	0.007	0.01	0.02	0.003	0.006
δ	0.056		0.055		0.050		0.053		0.056		0.053	
+/- Δ_δ	0.011	0.006	0.007	0.006	0.006	0.008	0.007	0.004	0.004	0.008	0.003	0.005
β	1.00											
+/- Δ_β	0.03						0.04					
γ	1.86											
+/- Δ_γ	0.13						0.09					
$S_{accMean}$	0.501		0.504		0.502		0.508		0.53		0.54	
+/- Δ_{Sacc}	0.011	0.006	0.009	0.017	0.014	0.008	0.003	0.004	0.04	0.03	0.04	0.02
$E_{accMean}$	0.72		0.36		0.19		0.043		0.004		-0.05	
+/- Δ_{Eacc}	0.03	0.02	0.05	0.02	0.06	0.04	0.016	0.016	0.011	0.001	0.05	0.16
R [Å]	43.6		56.2		66		86		129		-	
+/- Δ_R [Å]	0.7	0.4	1.0	0.8	3	2	6	1	42	17	-	-

bioRxiv preprint doi: https://doi.org/10.1101/2023.12.29.573596; this version posted December 29, 2023. The copyright holder for this preprint (which was not certified by peer review) is the author/funder, who has granted bioRxiv a license to display the preprint in perpetuity. It is made available under aCC-BY-NC-4.0 International license.

Supplementary Table 10: Accurate FRET analysis of DNA Cy3B-Cy5 measured on a standard confocal microscope. Correction factors for leakage α, direct excitation δ, detection corrections β and γ and accurate FRET values and calculated distances.

bp	**8**	**13**	**18**	**23**	**28**	**33**
α	0.12	0.12	0.12	0.12	0.13	0.12
δ	0.07	0.07	0.07	0.07	0.07	0.06
β	0.94					
γ	0.54					
E_{acc}	0.96	0.77	0.54	0.25	0.12	0.07
σ_{Eacc}	0.03	0.08	0.09	0.12	0.09	0.08
S_{acc}	0.51	0.48	0.49	0.52	0.52	0.51
σ_{Sacc}	0.08	0.08	0.09	0.09	0.09	0.08
R_0 [Å]	73.7					
distance [Å]	43.1	60.4	71.7	88.2	103	114

Supplementary Table 11: Accurate FRET analysis of DNA Cy3B-Atto647N measured on a standard confocal microscope. Correction factors for leakage α, direct excitation δ, detection corrections β and γ and accurate FRET values and calculated distances.

bp	**8**	**13**	**18**	**23**	**28**	**33**
α	0.12	0.12	0.12	0.12	0.12	0.12
δ	0.04	0.02	0.02	0.04	0.04	0.04
β	0.95					
γ	0.82					
E_{acc}	0.91	0.67	0.46	0.21	0.12	0.06
σ_{Eacc}	0.04	0.08	0.09	0.08	0.06	0.06
S_{acc}	0.50	0.50	0.51	0.50	0.50	0.50
σ_{Sacc}	0.07	0.07	0.08	0.08	0.07	0.08
R_0 [Å]	67.0					
distance [Å]	45.2	59.7	68.8	83.4	93.3	105

bioRxiv preprint doi: https://doi.org/10.1101/2023.12.29.573596; this version posted December 29, 2023. The copyright holder for this preprint (which was not certified by peer review) is the author/funder, who has granted bioRxiv a license to display the preprint in perpetuity. It is made available under aCC-BY-NC 4.0 International license.

Supplementary Table 12: Accurate FRET analysis of DNA Cy3-Atto647N measured on a standard confocal microscope. Correction factors for leakage α, direct excitation δ, detection corrections β and γ and accurate FRET values and calculated distances.

bp	**8**	**13**	**18**	**23**	**28**	**33**
α	0.09	0.10	0.12	0.10	0.09	0.10
δ	0.04	0.04	0.04	0.04	0.04	0.04
β	1.09					
γ	2.97					
E_{acc}	0.77	0.39	0.18	0.06	0.03	-0.04
σ_{Eacc}	0.09	0.09	0.06	0.05	0.04	0.06
S_{acc}	0.51	0.50	0.50	0.51	0.50	0.51
σ_{Sacc}	0.07	0.07	0.07	0.07	0.08	0.09
R_0 [Å]	51.1					
distance [Å]	41.9	54.9	65.5	80.4	91.8	-

Supplementary Table 13: Comparison of correction factors β and γ of the BRICK-MIC and a standard confocal microscope.

	DNA-Cy3B-Atto647N		**DNA-Cy3B-Cy5**		**DNA-Cy3-Atto647N**	
	Standard Confocal	**BRICK-MIC**	**Standard Confocal**	**BRICK-MIC**	**Standard Confocal**	**BRICK-MIC**
β	0.95	1.00	0.94	0.90	1.09	1.00
γ	0.82	0.51	0.54	0.32	2.97	1.86

bioRxiv preprint doi: https://doi.org/10.1101/2023.12.29.573596; this version posted December 29, 2023. The copyright holder for this preprint (which was not certified by peer review) is the author/funder, who has granted bioRxiv a license to display the preprint in perpetuity. It is made available under aCC-BY-NC-4.0 International license.

Supplementary Table 14: E*-S*-fit results of MalE (T36C-S352) labelled with Alexa555-Alexa647 measured with Brick-MIC and standard confocal microscope.

	Brick-MIC		Standard confocal	
$c_{maltose}$ [mM]	0	1	0	1
E*	0.57	0.76	0.68	0.84
σ_{E^*}	0.08	0.07	0.07	0.05
S*	0.49	0.53	0.46	0.51
σ_{S^*}	0.06	0.06	0.06	0.06

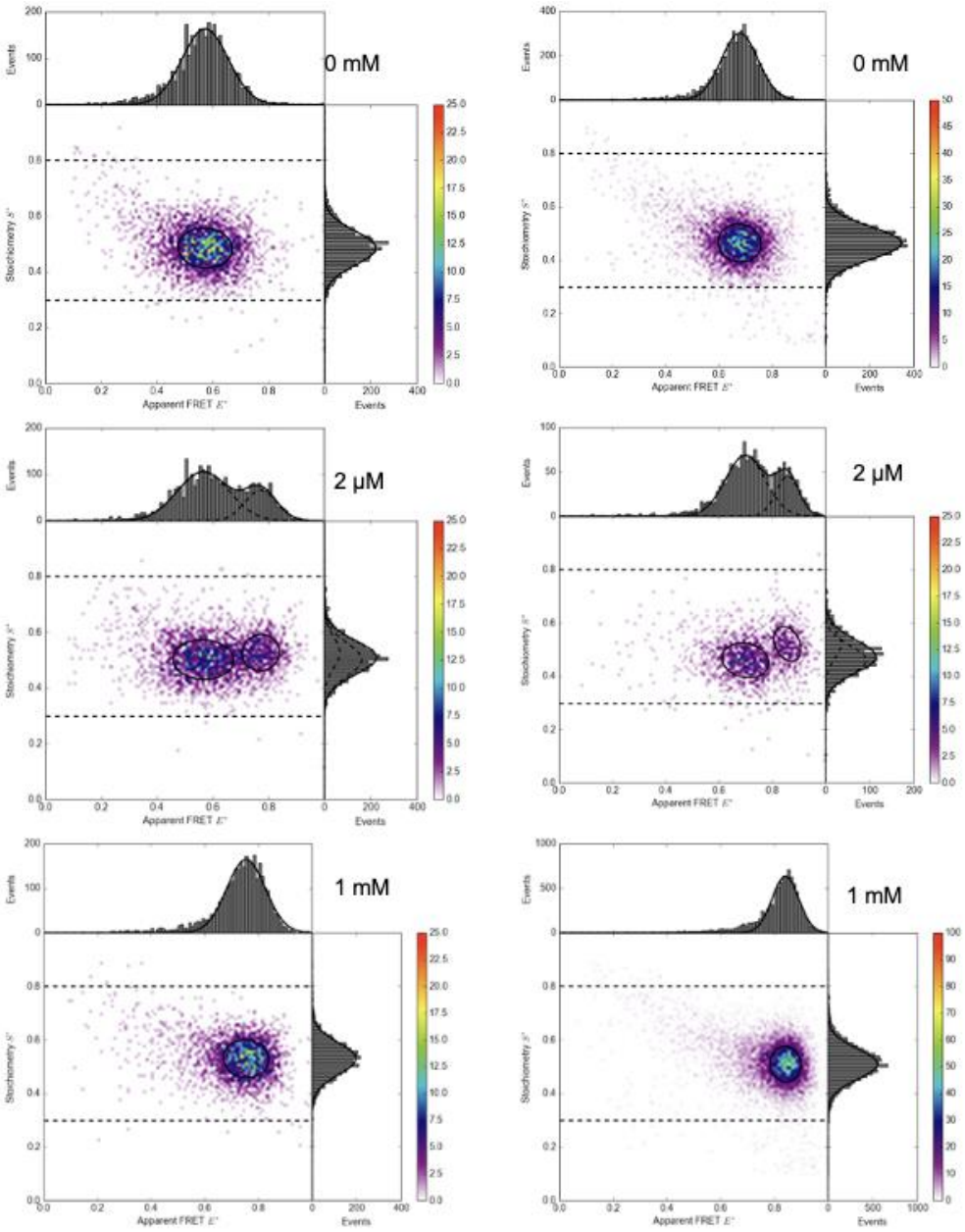

Supplementary Fig. 12: ES-histograms of MalE (T36C-S352) labelled with Alexa555-Alexa647 measured with Brick-MIC (left) and a standard confocal microscope (right). ES-histograms for maltose concentrations 0 mM, 2 µM and 1 mM, reflecting the apo, KD and holo states, respectively.

bioRxiv preprint doi: https://doi.org/10.1101/2023.12.29.573596; this version posted December 29, 2023. The copyright holder for this preprint (which was not certified by peer review) is the author/funder, who has granted bioRxiv a license to display the preprint in perpetuity. It is made available under aCC-BY-NC 4.0 International license.

Supplementary Table 15: Accurate FRET analysis of MalE (T36C-S352) labelled with Alexa555-Alexa647, measured with Brick-MIC (left) and a standard confocal microscope (right). Using the correction factors α, δ, β and γ accurate FRET values and the distances for the opened and closed conformation, apo and holo state, respectively, of MalE (T36C-S352) were calculated. The Förster radius for Alexa555 and Alexa647 R_0 = 51 Å. *DD and AA only E- and S- values were determined from data sets with a significant DD- and AA-only population with the same protein and fluorophore.

	Brick-MIC, ALEX				**Standard confocal microscope**	
$c_{maltose}$[mM]	**0**		**1**		**0**	**1**
α	0.060		0.0578		0.10*	
+/- Δ_α	0.004	0.003	0.0003	0.0003	-	-
δ	0.082		0.092		0.07*	
+/- Δ_δ	0.011	0.013	0.007	0.008	-	-
β	0.83				0.82	
+/- Δ_β	0.04		0.08		-	-
γ	1.82				2.34	
+/- Δ_γ	0.15		0.09		-	-
$S_{accMean}$	0.493		0.499		0.50	0.49
+/- Δ_{Sacc} -	0.004	0.005	0.003	0.003	-	-
$E_{accMean}$	0.36		0.62		0.39	0.66
+/- Δ_{Eacc}	0.01	0.03	0.03	0.04	-	-
R [Å]	56.2		47.2		54.9	45.7
+/- Δ_R [Å]	0.5	0.5	0.4	1.1	-	-

Supplementary Table 16: Comparison of measured and simulated distances of the conformational states of MalE (T36C-S352) labelled with Alexa555-Alexa647. All distances in the table provided in Å.

Conformational state of MalE1	**Apo**	**Holo**
AV calculations	57.5	46.3
Brick-MIC	56.2	47.2
Standard confocal	54.9	45.7

bioRxiv preprint doi: https://doi.org/10.1101/2023.12.29.573596; this version posted December 29, 2023. The copyright holder for this preprint (which was not certified by peer review) is the author/funder, who has granted bioRxiv a license to display the preprint in perpetuity. It is made available under aCC-BY-NC 4.0 International license.

Brick-MIC components list

	Components	Company	Product number	µFCS	µALEX	µEpi
Light source/detection	Lasers diode	Thorlabs	CPS532	✓		
		Coherent	OBIS 532-100- LS		✓	
			OBIS 640-100-LX		✓	
		Fisba	READY Beam™ ind 2 1007773			✓
	Photomultiplier (PMT)	Hamamatsu	H10682-210	✓		
			H10682-01	✓		
	Avalanche photo diode (APD)	MPD	PDM 50-Micron		✓(x2)	
	CMOS camera	IDS	U3-30C0CP-M-GL rev.2.2			✓(x2)
	Photon counting module	National Instruments	BNC-2121 (778289-01)		✓	
		Measurement Computing	USB-CTR04	✓		
Optics / Mechanics	Objective	Olympus	UPLSAPO60XW	✓	✓	
			UPLSAPO60XO			✓
	Piezo mount	Newport	AG-M100N	✓(x2)	✓(x2)	✓
	Piezo controller		AG-UC2	✓	✓	✓
	Mirrors	Thorlabs	PF10-03-G01	✓ (x3)	✓ (x3)	✓ (x2)
	Mirror mount		KM100	✓	✓ (x2)	✓
	Reflective Collimator mount		KM100T		✓	
	Reflective Collimator		RC04APC-P01			✓
			RC12APC-P01		✓	
			RC12FC-P01	✓		
	Fixed focus Collimator		F220FC-532	✓		
	Optical fiber		M67L01	✓		
			M64L01	✓		
			P1-980AFC-1	✓		
			P1-630AFC-1	✓		
			P5-488PM-FC-2		✓	
	Lenses		AC254-200-A		✓	
			AC254-150-A-ML			✓
			LC1054-ML - Ø1/2			✓
			LA1134-A-ML - Ø1			✓
			LA1433-A-ML - Ø1		✓	
		Newport	KBC043AR.14		✓	
	Manual Z-stage		MR5.16 C01-338066	✓	✓ (x3)	✓ (x3)
Filters	DIC	Chroma	ZT532/640rpc 25.5 x 36 x 2 mm	✓	✓	✓
			ZT640rdc 25.5 x 36 x 1 mm	✓	✓	
			ZT640rdc 25.5 x 36 x 2 mm			✓
	Bandpass		ET700/75m ⌀25 mm	✓	✓	✓
		Semrock	FF01-582/75-25 ⌀25 mm	✓	✓	✓
	Clean-up	Chroma	ZET 635/10 ⌀25 mm		✓	✓
			ZET 532/10 ⌀25 mm		✓	
		Thorlabs	FL05532-10 ⌀12.5 mm	✓		
	ND		NDC-50C-2M	✓		✓
minor	M4 Nutt	Generic		✓ (x6)	✓ (x6)	✓ (x8)
	M3 Nutt			✓ (x3)	✓ (x3)	✓ (x3)
	M4 15 mm screw					✓ (x4)
	M4 8 mm screw			✓ (x6)	✓ (x14)	✓ (x4)
	M3 15 mm screw			✓ (x2)		
	M3 12 mm screw			✓ (x2)		✓ (x1)
	M3 10 mm screw			✓ (x8)		
	M3 5mm screw			✓ (x4)	✓ (x12)	✓ (x14)
	M2.5 5mm				✓ (x10)	
	ball bearing		10 mm outside Ø, 3 mm inside Ø, 4mm width	✓ (x3)	✓ (x3)	✓ (x3)
	Magnet 8 mm Ø x 1 mm			✓ (x4)	✓ (x4)	
	Magnet 5 mm Ø x 2 mm					✓ (x24)